Energy Conversion and Management 263 (2022) 115718

Contents lists available at ScienceDirect

Energy Conversion and Management

journal homepage: www.elsevier.com/locate/enconman

Investigation of an integrated circulating fluidized bed gasifier/steam turbine/proton exchange membrane (PEM) fuel cell system for torrefied biomass and modeling with artificial intelligence approach

Furkan Kartal, Uğur Özveren *

Department of Chemical Engineering, Marmara University, Goztepe Campus, 34722, Kadikoy, Istanbul, Turkey

ARTICLE INFO

Keywords:
PEM fuel cell
Gasification
CFB gasifier
Torrefied biomass
ANN

ABSTRACT

In this study, the Aspen Plus simulator was used to develop a circulating fluidized bed (CFB) gasifier/steam turbine/proton-exchange membrane (PEM) fuel cell integrated system. Since integrated systems comprise many thermochemical, biochemical, and physical processes, equipment, chemicals, etc., determining output parameters is challenging and important. In this context, twenty torrefied biomass samples were parametrically analyzed for syngas properties and H_2 production rates. So, using solid fuel characteristics and gasifier operating parameters, a data set including PEM fuel cell module outputs was created. Thereafter, the created data set was utilized to train the artificial neural network (ANN) model. This paper, as far as we know, examines the impacts of different torrefied biomass samples on PEM fuel cell outputs for a sophisticated integrated system dependent on gasification conditions, and provides a more generalized and rapid prediction model for the integrated system with complicated equations. Additionally, parametric studies assist in determining the proposed new integrated system's minimal operating condition, which is highly dependent on the fuel characteristic.

High steam/fuel ratio, high carbonization degree, and low pressure lowered PEM efficiency while increasing power and voltage outputs. The ANN model also accurately forecasts PEM fuel cell output parameters (R^2 greater than 0.99 and MAPE less than 1%) based on torrefied biomass proximate analysis data and gasification process operating parameters. As a consequence, a CFB gasifier/steam turbine/PEM fuel cell system, which contains diverse modules and thermochemical processes, can be examined using ANN models trained on a large and high-quality dataset.

1. Introduction

Renewable energy sources including solar, wind, hydropower, and biomass are particularly appealing for developing sustainable and low carbon energy systems. Among them, biomass is the world's oldest known energy source and the only carbon-based source that is not fossil. Biomass-based renewable energy is clean, safe, and beneficial for protecting the environment, the economy, and energy security [1]. Biomass has several advantages, including CO_2 neutrality and its worldwide occurrence. And unlike wind and solar energy, it does not suffer from the problem of intermittent availability. Despite these benefits, raw biomass has a number of inherent flaws that restrict its widespread usage and directly impact its cost [2]. Due to biomass' low energy density, cogeneration, thermochemical, and biochemical conversion facilities need huge volumes of biomass, causing storage, transportation, and handling issues. The high moisture content leads to uncertainties in the physical, chemical, and microbiological properties of the biomass. When feeding a gasification or co-incineration plant, irregularities in the shape of the biomass are another problem. To overcome these challenges to the raw biomass and make it suitable for energy applications, the biomass must undergo pretreatment processes [3].

Torrefaction is a thermal pretreatment technique that involves moderate pyrolysis of biomass in an inert, oxygen-free environment around 200–300 °C [4,5]. Torrefaction enhances biomass calorific value and energy density. Biomass can also be converted less hygroscopic and more hydrophobic, improving its storage stability. The decomposition processes that occur at the temperature of torrefaction increase the grindability of biomass by thoroughly drying it out and removing its unruly and fibrous structure [5,6]. Moreover, depending on the torrefaction circumstances, torrefied biomass turns brown to dark brown and

* Corresponding author.
E-mail address: ugur.ozveren@marmara.edu.tr (U. Özveren).

https://doi.org/10.1016/j.enconman.2022.115718
Received 25 March 2022; Received in revised form 26 April 2022; Accepted 2 May 2022
Available online 12 May 2022

has qualities similar to coal [6]. All these changes allow better performance of biomass by improving its physical, chemical and biochemical composition, making it a very attractive option for gasification applications.

Gasification is the thermochemical conversion of organic matter into combustible gases with reduction of oxygen below the stoichiometric amount required for complete combustion [7]. Since this process converts a difficult-to-handle solid into a gaseous product that is simple and affordable to handle, and can be readily refined into a feedstock for the synthesis of other chemicals or clean fuels, it can be labelled refining [8]. Furthermore, a syngas with the appropriate composition can be fed into an additional cycle at high temperatures, resulting in a more efficient gasification process [9] that generates more power and provides a cost-effective method in integrated plants. In this context, gas turbine technology has advanced significantly in recent years, due to the implementation of solid fuel gasifiers [10]. Various studies for the investigation of the effect of torrefaction of biomass on the gasification parameters and performance are available in the literature [11–13]. Pinto et al. [11] studied the effects of torrefaction, densification, and densification after torrefaction on eucalyptus stump gasification performance, quality, and yield. Pretreated samples were gasified into syngas in a fluidized bed reactor and compared to raw stumps. Torrefied biomass enhances syngas output and cold gas efficiency while decreasing tar production. Chen et al. [13], numerically gasified high volatile bituminous coal, and raw and torrefied bamboo and compared them. Torrefied bamboo outperforms raw bamboo in gasification and is equivalent to coal gasification. However, multiple studies have previously been published on steam gasification of torrefied biomass [14–18]. Steam gasification provides much better gas quality than gasification with air, especially in small and medium scale. The method is especially favorable for turning biomass into second-generation fuels like Fischer-Tropsch diesel, methanol, dimethyl ether (DME), or substitute natural gas (SNG) [19].

Fundamental design features of novel gasifiers that utilize solid carbonaceous fuel (particles) must be carefully assessed. Because chemical and physical processes in gasifiers are complicated, experimental research cannot usually define all relevant phenomena [20,21]. Simulation of the gasification process saves resources and time by forecasting behavior and analyzing parameters. Aspen Plus, a product of AspenTech, is the most widely used program in the literature for gasification process simulation studies [22,23]. The program forecasts dynamic responsiveness, performance, and economic feasibility based on thermodynamic features of any process. Aspen Plus has been used in several research studies to model and simulate the gasification of torrefied biomass [24–26]. On the other hand, CFB gasification studies of torrefied biomass used in Aspen Plus are limited [27]. ANN models, in addition to process simulators, are well-established techniques for estimating or optimizing parameters in gasification processes [28,29], fuel cells [30,31], and other integrated systems [32,33]. Pashchenko [34] researched two different approaches for a thermochemical waste-heat recovery system based on coal gasification: steam gasification and steam-flue gas mix gasification. The author used the Aspen HYSYS simulator to assess the efficiency of coal gasification thermochemical recovery systems. The findings show that heat recovery is greatest at 720 °C for a steam/carbon ratio of 1.0, 810 °C for a steam/carbon ratio of 0.5, and 930 °C for a steam/carbon ratio of 0.25. Shahavi et al. [35] used a newly proposed combined cycle based on waste gasification integrated with low-temperature air separation, gas turbine, and CO_2 power generation cycle by comparing seven agricultural wastes for renewable heat and power generation. Using the Aspen Plus process simulator, the researchers performed thermodynamic analysis to estimate different plant parameters such as cold gas efficiency, carbon conversion efficiency, renewable power capacity, and so on. Moreover, Behzadi et al. [36] presented a biomass-fired PEM fuel cell with an organic Rankine cycle and thermoelectric generator that uses several gasification agents for power and heat generation as well as hot water production. The authors conducted a parametric analysis to assess the impact of important potential determinants on CO_2 emission index, energy and exergy efficiencies, output power, and total cost rate, and then used the genetic algorithm approach in MATLAB software to further optimize parameters. Various software programs are used to determine and optimize the parameters of solid-fuel-based combined cycles in the literature. However, no thermodynamic analysis for a CFB gasifier/steam turbine/PEM fuel cell system based on torrefied biomass characteristic and gasification condition has been completed to date, and no study has published on estimating PEM output variables using simulation data.

When a mathematical equation or model is absent, or when the model is too sophisticated for practical applications, ANN is an effective instrument. ANN is a particularly effective tool because of its capacity to learn from simulation or experimental data. As a result, it is used in a wide variety of engineering applications [37–40]. In addition, it is known that ANNs are powerful models that provide better results when the dataset is large [41], and considering that the integrated system presented in this study includes complex equations (Sections 2.2 and 2.3), it seems appropriate to prefer the ANN model.

One of the most promising of the numerous combined process methods for producing electricity from syngas is fuel cell-based integrated combine systems. Solid fuel processing could benefit from combining the fuel cell and gasification processes to provide high efficiency small-scale power [42]. Fuel cells are electrochemical devices that transform chemical energy directly into electrical energy, producing water as a by-product [43]. Due to their low pollution, simple system designs, and absence of moving parts, fuel cells are widely acknowledged as a leading candidate for power generation [44]. The PEM fuel cell has a number of advantages over conventional energy conversion technologies, including low operating temperature (high temperature PEM fuel cells operate at 120–200 °C and low temperature PEM fuel cells operate at 60–80 °C), low or zero noise, low emissions, light weight, rapid commissioning time (less than 30 s), quick response to load changes, and high efficiency and power density [44,45]. There have already been previous studies in which the experimental analysis of the integration of the PEM fuel cell with the biomass-fed gasification process [46], and the models for the integrated system are simulated in Aspen Plus [47–50], but, there are no publications in the literature that examine the integration of torrefied biomass gasification combined with a PEM fuel cell in Aspen Plus.

In this study, for the first time, a CFB gasifier, a steam turbine, and a PEM fuel cell were integrated for the gasification of torrefied biomass with varying fuel characteristics using Aspen Plus software. The performance of this simulated system was examined depending on the operation conditions of the gasification process, and both energy and exergy analysis were performed. Another novelty of this study is the investigation of the effects of CFB gasifier operating conditions and torrefied biomass fuel properties on PEM fuel cell power, voltage, and performance using an ANN model, which is an artificial intelligence approach. Thus, using an ANN model trained with simulation data generated by an integrated model based on thermodynamic equilibrium, output parameters for a complex plant can be determined quickly and accurately.

2. Methodology

2.1. Feedstock Characterization

The torrefied biomass samples used in this study's thermodynamic equilibrium calculations were collected by literature review. The feedstock materials were torrefied at various temperatures (240 °C, 250 °C, 270 °C, 275 °C, 300 °C, etc.) for various durations (15 min, 30 min, 60 min, etc.) in an inert environment. The ultimate and proximate analysis findings of the samples are listed in Table 1.

When the proximate analysis findings of the torrefied materials are

Table 1
Proximate and ultimate analysis results (wt.%) of the torrefied biomass samples.

Sample	Proximate Analysis				Ultimate Analysis				
	Moisture	Fixed Carbon	Volatile Matter	Ash	C	H	O	N	S
Olive kernel [51]	4.00	37.80	54.30	3.90	63.40	5.20	26.50	1.00	0.10
Hardwood [52]	3.80	28.00	72.00	1.60	58.40	5.70	35.80	0.00	0.00
Willow [52]	3.80	27.60	72.40	0.70	56.90	5.90	37.30	0.00	0.00
Eucalyptus [52]	4.30	28.80	71.20	2.00	61.90	5.80	32.30	0.00	0.00
Teak [53]	2.74	41.28	54.20	1.78	60.40	5.67	31.56	0.35	0.21
Melina [53]	2.68	41.06	54.09	2.17	66.05	5.18	26.02	0.36	0.22
Wheat straw [54]	0.30	26.40	65.20	8.40	51.90	5.90	33.20	0.80	0.00
Reed canary grass [54]	1.30	16.10	76.60	7.30	52.20	6.00	37.30	0.10	0.00
Empty fruit bunch [55]	7.68	30.15	54.50	7.67	47.65	6.63	39.60	5.62	0.53
Loblolly pine chips [56]	6.32	20.80	78.60	0.60	55.00	5.94	38.30	0.11	0.00
Palm kernel shells [57]	4.67	37.27	54.72	8.01	53.91	5.37	31.82	0.89	0.00
Norwegian Spruce [58]	3.79	23.41	72.34	0.46	52.72	5.88	40.86	0.06	0.03
Norwegian forest residues [58]	4.17	31.47	61.63	2.73	56.84	5.51	34.29	0.61	0.06
Switchgrass [59]	2.05	27.50	67.52	4.98	59.16	4.67	34.53	0.44	1.20
Juniper [60]	5.69	18.63	74.60	1.08	53.60	5.42	34.10	0.19	0.01
Mesquite [60]	4.84	23.27	69.50	2.39	53.40	5.33	33.20	0.81	0.05
Bamboo forest residues [61]	5.07	24.52	48.39	22.02	48.63	4.76	16.73	1.65	0.14
Poultry litter [62]	5.22	22.61	48.56	23.61	38.78	5.15	51.49	4.01	0.57
Pigeon pea stalk [63]	2.09	44.87	49.59	3.45	53.82	6.62	38.85	0.71	0.00
Pine wood chips [64]	1.90	40.93	55.67	1.50	65.29	5.94	28.46	0.28	0.03

evaluated, the most notable results are an increase in fixed carbon content and a reduction in volatile matter content. Nevertheless, the volatile matter and fixed carbon content vary depending on the characteristics of the raw biomass and the operational conditions of the torrefaction procedure. It is possible to observe a torrefied biomass sample with a volatile matter composition of more than 70%. Similar to the biomass, torrefied materials normally have a low ash concentration, although bamboo forest residues and poultry litter samples had ash content of more than 20%. Despite the fact that the torrefaction process is known to increase ash concentration in solid materials, the increase was not in significant level owing to the low ash percentage of the raw material. The impact of thermal pretreatment on the elemental structure of solid materials, on the other hand, can be observed more clearly. The Van Krevelen diagram [65] is a technique for recognizing solid fuels and, in particular, determining their carbonization degree. The H/C and O/C ratios can be used to determine if a solid fuel belongs to a given class, and data on its quality can be acquired. Fig. 1 depicts the Van Krevelen diagram for the torrefied biomass samples used in this paper.

The high O/C and H/C values in biomass samples imply that they are solid fuels with low calorific value [66]. As indicated in Fig. 1, the O/C ratio for biomass is between 0.4 and 0.9, whereas the H/C ratio is between 1.2 and 1.6. Torrefaction is a thermochemical process that decreases the O/C and H/C ratios and by enriching the solid fuel's C content and lowering the H and O content. The majority of the torrefied biomass samples in this research were also identified in the peat zone, which stands between biomass and lignite. In other words, in terms of carbonization degree, the majority of torrefied samples are higher-quality fuels than biomass. Furthermore, materials with a higher degree of carbonization, such as melina, olive kernel, pine wood chips, and bamboo forest residues, are observed in the lignite region, while torrefied materials with high H/C and O/C ratios, such as empty fruit bunch and poultry litter, are found outside of the biomass zone. Therefore, the raw material's physicochemical properties have a substantial impact on the carbonization degree of the torrefied material.

2.2. Thermodynamic equilibrium modeling

Through planning, operation, design, and troubleshooting, a better

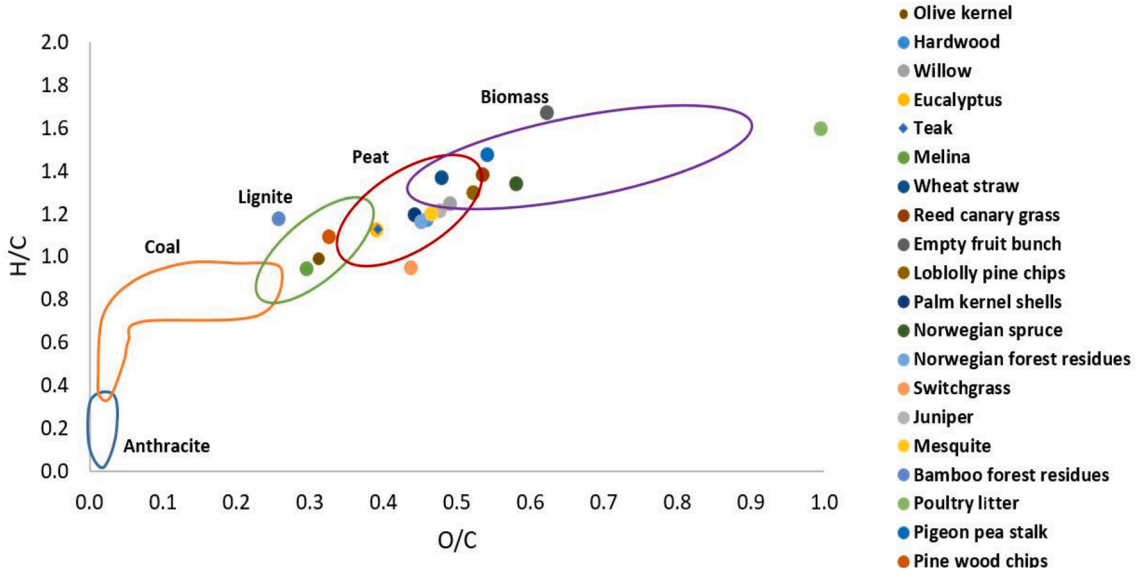

Fig. 1. Characterization of torrefied biomass samples by Van Krevelen diagram.

knowledge of the whole process may assist to decrease impediments and, as a consequence, boost the plant's economic competitiveness [67]. Mathematical models are statements that are dependent on rates or equilibria, and they frequently include calculations for mass and energy balances. The most basic technique is thermodynamic equilibrium, which posits that substances continuously react with one another indefinitely until an equilibrium is reached. The validity of the suggested model and the correctness of the essential thermochemical parameters define the thermodynamic modeling's performance [68]. There are two methods for computing thermochemical equilibrium from a thermodynamic approach. One method is to use the equilibrium constant methodology, which requires both understanding of the relevant chemical process and calculation of the equilibrium constant. Second, the Gibbs energy minimization technique which does not need knowledge of the fundamental chemical processes for estimating the thermochemical equilibrium [69]. According to the second rule of thermodynamics, the Gibbs energy of the system reaches its minimum value at a given temperature and pressure when the system reaches equilibrium, and the components of feedstock material are equilibrium compositions that follow the law of matter conservation [70]. The total Gibbs energy of the system is given by,

$$G^{t}_{T,P} = g(n_1, n_2, n_3, \cdots, n_i) \tag{1}$$

where the overall Gibbs energy of the system is denoted by $G^{t}_{T,P}$ whereas each species is denoted by n_i. The objective is to identify a configuration of n_i that minimizes the system's overall Gibbs energy. To do this, a series of approaches can be used. The first step is to determine how much material is in each of the system's components,

$$\sum_i n_i a_{ik} = A_k (k = 1, 2, \cdots, w) \tag{2}$$

where A_k is the total number of atomic masses of the k_{th} element in the system, a_{ik} is the number of atoms of the k_{th} element in each molecule of the chemical species i, and w is the total number of atoms in the system. The next process is to sum over the range of k in Eq. (2) to add Lagrange multipliers (λ_k).

$$\sum_k \lambda_k \left(\sum_i n_i a_{ik} - A_k \right) = 0 \tag{3}$$

Combining Eqs. (1) and (3), a new equation can be expressed as,

$$F = G^{t}_{T,P} + \sum_k \lambda_k \left(\sum_i n_i a_{ik} - A_k \right) \tag{4}$$

The above equation is identical to Eq. (1) if the second component on the right side is equal to zero. F achieves its minimum value when the partial derivative with respect to each specie approaches zero at a given temperature and pressure,

$$\frac{\partial F}{\partial n_i} = \frac{\partial G^{T}}{\partial n_i} + \sum_k \lambda_k a_{ik} = 0, (i = 1, 2, \cdots, n) \tag{5}$$

Since the chemical potential μ_i is the first term on the right hand side of the equation, Eq. (5) can be written as,

$$\mu_i + \sum_k \lambda_k a_{ik} = 0 \tag{6}$$

The chemical potential can be expressed as follows:

$$\mu_i = G^{0}_{i} + RTln\left(\frac{f_i}{f^{0}_{i}}\right) \tag{7}$$

where $G^{0}_{i} = \Delta G^{0}_{fi}$ is the Gibbs energy of formation in the standard state, R is the universal gas constant, T is the temperature, and f is the species' fugacity. The fugacity ratio could be substituted with the species' mole faction if all gases are considered to be ideal gases at standard pressure,

$$\mu_i = \Delta G^{0}_{fi} + RTln\left(\frac{n_i}{n_{total}}\right) \tag{8}$$

When the above equation is inserted into Eq. (5),

$$\Delta G^{0}_{fi} + RTln\left(\frac{n_i}{n_{total}}\right) + \sum_k \lambda_k a_{ik} = 0, (i = 1, 2, \cdots, n) \tag{9}$$

According to the aforementioned equation, the n equilibrium equation relates to each species in the system. Hence, for each species present in the system, one equation is selected from Eq. (9) and the remaining equations for the Langrange multiplier are obtained from the mass constraint equations.

2.3. PEM fuel cell modeling

Aspen Custom Modeler (ACM) already has a model for the PEM procedure. Fuel cell calculations are included in the custom model, which are accessible in the literature by Yi and Nguyen [71], as well as steady-state mass and energy balance formulae. A two-dimensional PEM fuel cell steady-state energy and mass model was created by the authors. The flow distributors, solid phases, cathode/anode flow channels, and membrane/electrode system are among the model components. A number of channels on both sides of the flow fields are accounted for, as is mass transfer of water and gas species inside the cell and heat transfer for gas/solid phases along flow channels. The mass and energy balances in the anode are as follows:

$$\frac{\partial Ma_{H_2}(x)}{\partial x} = -\frac{hI(x)}{2F} \tag{10}$$

$$\frac{\partial Ma^{L}{}_{H_2O}(x)}{\partial x} = \left\{ \frac{k_c hd}{R[T(x) + 273.15]} \right\} \left\{ \frac{Ma^{V}{}_{H_2O}(x)}{Ma^{V}{}_{H_2O}(x) + Ma_{H_2}(x)} \left(Ppa_{H_2O}(x) - Pa_{sat}(x) \right) \right\} \tag{11}$$

$$\frac{\partial Ma^{V}{}_{H_2O}(x)}{\partial x} = -\frac{\partial Ma^{L}{}_{H_2O}(x)}{\partial x} - \frac{ha(x)}{F} I(x) \tag{12}$$

$$\left(Ma_{H_2}(x) + Ma^{V}{}_{H_2O}(x) + Ma_{inert}(x) \right) Cp \frac{\partial T(x)}{\partial x} = Ua(T_s(x) - T_a(x)) \tag{13}$$

where subscripts *a*, *inert* and *sat* represent anode, inert gas and saturation, respectively, while superscripts *L* and *V* represent liquid and vapor phases, respectively. M_i is molar flow rate (mol/s) of species i, x is direction along the channel length (cm), h is channel width (cm), $I(x)$ is local current density (A/cm^2), F is Faraday constant, k_c is condensation rate constant (s^{-1}), h is channel width (cm), d is channel height (cm), Ppi is the partial pressure of species i (atm), Cp is the heat capacity of the heat exchanger fluid (J/mol.°C), $a(x)$ is the heat-transfer length per unit area between the channel and the solid layer (cm), U is overall heat-transfer coefficient between channel and solid layer (J/(s.cm^2.°C)), and $T(x)$ is temperature of a stream (°C). The mass and energy balances in the cathode are also stated as:

$$\frac{\partial Mc_{O_2}(x)}{\partial x} = -\frac{hI(x)}{4F} \tag{14}$$

$$\frac{\partial Mc^{L}{}_{H_2O}(x)}{\partial x} = \left\{\frac{k_c hd}{R[T(x)+273.15]}\right\}\left\{\frac{Mc^{V}{}_{H_2O}(x)}{Mc^{V}{}_{H_2O}(x)+M^{L}{}_{O_2}(x)+Mc_{inert}(x)}\right\}(Pc(x)-Pc_{sat}(x)) \tag{15}$$

$$\frac{\partial Mc^{V}{}_{H_2O}(x)}{\partial x} = -\frac{\partial Mc^{L}{}_{H_2O}(x)}{\partial x}+\frac{h(1+2a(x))I(x)}{2F} \tag{16}$$

$$\left(Mc_{O_2}(x)+Mc^{V}{}_{H_2O}(x)+Mc_{inert}(x)\right)Cp\frac{\partial T(x)}{\partial x} = Ua(T_s(x)-T_c(x)) \tag{17}$$

where subscript c represents cathode side of the fuel cell. The energy balance in the solid layer is as follows:

$$\begin{aligned} A_{sol}k_s\frac{\partial^2 T(x)}{\partial x^2} - n_c\left(Ma^{L}{}_{H_2O}(x)+Mc^{L}{}_{H_2O}(x)\right)Cp_{H_2O}\frac{\partial T(x)}{\partial x} = & -n_c Ua(T_a(x) \\ & +T_c(x)-2T_s(x))-A_bU_b\left(T_{hef}(x)-T_s(x)\right)-n_c\left\{H^{V}_{H_2O,a} \right. \\ & \left. -H^{L}_{H_2O,a}\right\}(x)\frac{\partial Ma^{L}{}_{H_2O}(x)}{\partial x}-n_c\left\{H^{V}_{H_2O,c}-H^{L}_{H_2O,c}\right\}(x)\frac{\partial Ma^{L}{}_{H_2O}(x)}{\partial x} \\ & +n_c h\left\{\left\{\frac{\Delta S_{H_2}}{2F}+\frac{\Delta S_{O_2}}{4F}\right\}\{T_s(x)+273\}-\eta(x)\right\}I(x) \end{aligned} \tag{18}$$

where the conductive heat-transfer area (cm^2) of a solid layer per unit area is written as A_{sob} n_c is number of channel for each side of membrane, the length (cm) of heat flux from the solid layer to the bulk per unit area is A_b (cm), U_b overall heat-transfer coefficient between solid layer and bulk or solid body and heat exchanger fluid (J/(s.cm^2.°C)), H_i is enthalpy (J/mol) of species i, ΔS_i change of entropy (J/(mol.K)) for the i species reaction on platinum, and $\eta(x)$ overpotential (V) for the oxygen reaction. Finally, the following are the current density and power values:

$$I_{avg} = \frac{1}{L}\sum\frac{\partial I(x)}{\partial x} \tag{19}$$

$$I(x) = \frac{condm(x)}{tm}(V_{oc}(x)-V_{cell}(x)-\eta(x)) \tag{20}$$

$$V_{stack} = V_{cell}N_{cell} \tag{21}$$

$$Power = I_{avg}V_{stack}N_c hL \tag{22}$$

where I_{avg} is average current density (A/cm^2), L is cell channel length (cm), $V_{oc}(x)$ is cell open-circuit potential (V), $V_{cell}(x)$ is cell potential (V), $condm(x)$ is membrane conductivity (S/cm), and tm is membrane thickness (cm). The following formulas are used to compute membrane conductivity and net water flux per proton flux:

$$condm(x) = (0.005139*wca(x)-0.00326)e^{\left(1268\left(\frac{1}{303}-\frac{1}{273.15+Ts(x)}\right)\right)} \tag{23}$$

$$\begin{aligned} a(x)I(x) = & n_d(x)I(x)-FD_w(x)\frac{(wc_c(x)-wc_a(x))}{1E5tm} \\ & -\frac{(wc_c(x)+wc_a(x))}{2}\frac{k_p}{(0.001ViscW)}F\frac{\left(Ppc_{H_2O}(x)-Ppa_{H_2O}(x)\right)1E5}{100tm} \end{aligned} \tag{24}$$

where D_w is effective diffusion coefficient (cm^2/s) of water in the membrane, wc is concentration of water (mol/cm^3) in the membrane, $n_d(x)$ is electro-osmotic drag coefficient, k_p is hydraulic permeability of water in membrane (cm^2), and $ViscW$ is water viscosity (g/(cm.s)).

2.4. Aspen Plus model description

Aspen Plus offers a comprehensive database of physical properties that may be used in simulation computations. Mass and energy flows are elements of process streams in the Aspen Plus. Aspen Plus divides material streams into three categories: mixed, conventional solids, and non-conventional solids (for heterogeneous solid materials). The Aspen Plus libraries are used to specify the thermodynamic properties of chemical components. Non-conventional components are identified using the solid component's proximate, ultimate, and sulfur analyses. The Soave-Redlich-Kwong equation of state is used, and the density and enthalpy of the torrefied biomass sample are determined using the DCOALIGT and HCOALGEN methods, respectively. In the modeling of the CFB gasifier model, several assumptions are taken into account: (i) H_2, CO_2, CO, CH_4, N_2, H_2O, NH_3, H_2S, HCl, NO_x, and SO_x molecules are produced during gasification; (ii) ash is considered inert; (iii) all activities in the gasification procedure achieve a state of equilibrium; (iv) complete char conversion occurs during gasification; (v) the gasifier model is in a steady state, with no changes in any of the parameters over time; (vi) in the unit blocks, there is no pressure drop. The Aspen Plus flowsheet diagram of the integrated system proposed in this work is shown in Fig. 2.

A non-conventional flow was assigned to the TBS feedstock material. The torrefied biomass sample's proximate and ultimate analyses were input as component properties of the stream TBS. The TBS stream is directed to the R0 block (RYield reactor), which transforms non-conventional substance into conventional compounds such as C, H_2, O_2, N_2, S, H_2O, and ash. This method was carried out by specifying the yield distribution using an external Fortran formulation applied to the R0 reactor block in the CALCULATOR module. The yield distribution shows how much of each component was produced throughout the non-conventional to conventional conversion process. Three different Gibbs reactors (RGibbs) were used to minimize Gibbs free energy and achieve thermodynamic equilibrium: R1, R2, and R3. Several reactors operating at different temperatures must be employed to produce an appropriate volume and composition of syngas. A single Gibbs reactor working at high temperatures, for example, accelerates endothermic processes, allowing CO_2 and CH_4 to be produced at far lower concentrations than in experimental tests. Therefore, at high temperatures, components produced at different temperatures should be avoided to some extent and instead incorporated directly in the producer gas (F8). The material flow between the Gibbs reactors was controlled using the CS1, CS2 and CS3 component splitter unit blocks. Component splitter blocks divide specified components into separate streams based on ratios. The producer gas was created by mixing the streams from the Gibbs reactors and component splitters in the MIX mixer block. The SPL2 unit block also transfers a part of the produced gas back to the R3 reactor, allowing gaseous products to be burned. The R3 reactor is a high-temperature Gibbs reactor that is fed a large quantity of oxygen. The CS3 block directs the oxygen to the F12 stream in order to avoid affecting the syngas composition due to the large quantity of oxygen provided. Additionally, the CS2 unit block also completes the conversion by feeding ash and any remaining unconverted carbon to R3. The solid particles (SOLIDPRT) in the produced gas are also separated using CYCLONE. The CS4 component splitter block eliminated even more undesirable elements from the F8, and also allowing the SYNGAS to be examined according to the standards (dry basis, dry-nitrogen free, etc.). The gasifying agent stream STEAM was separated into two streams (ST1 and ST2) and given to the Gibbs reactors at different percentages in the splitter block STMSPL.

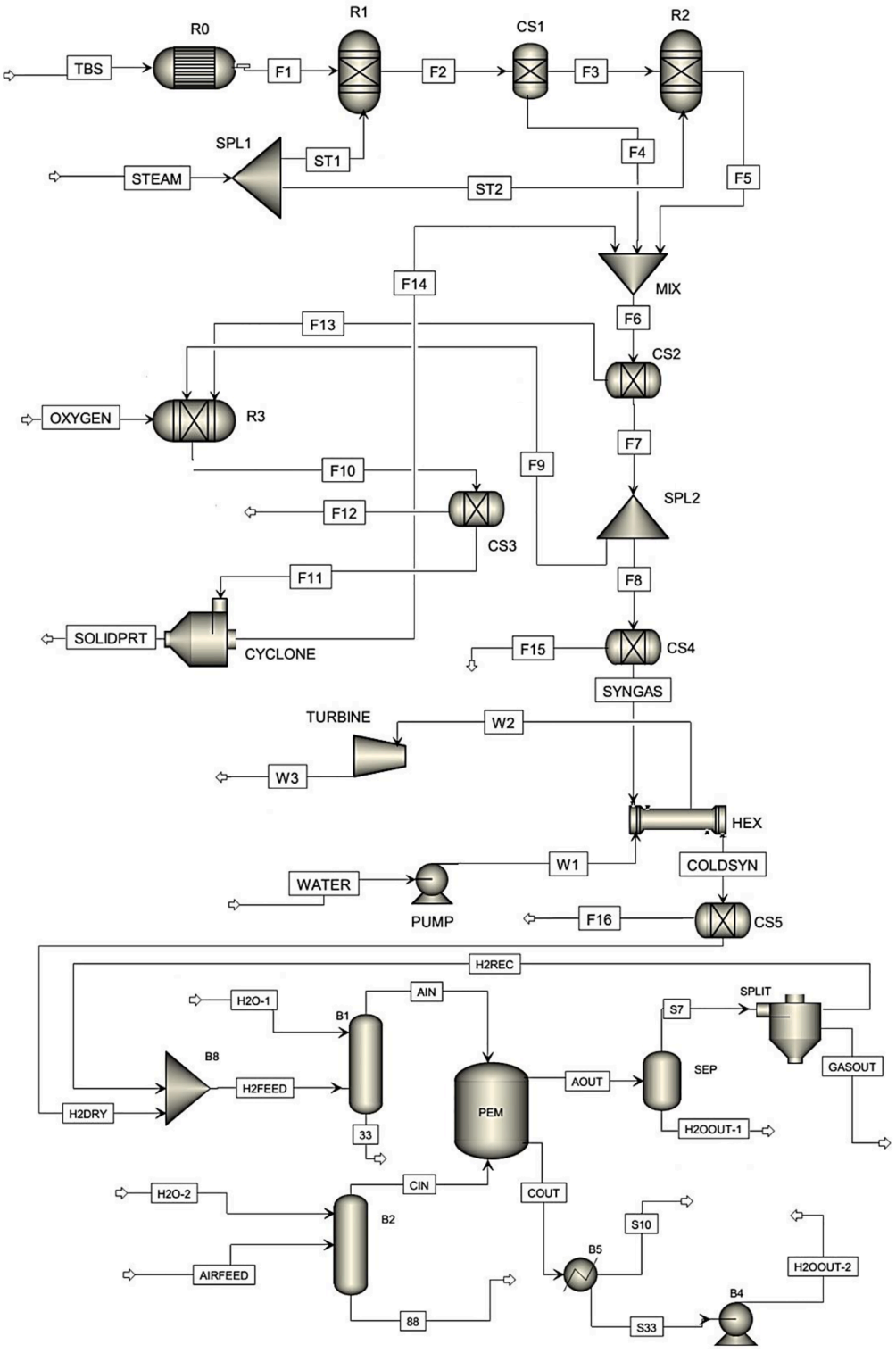

Fig. 2. Aspen Plus flowsheet diagram of the combined CFB gasifier/steam turbine/PEM fuel cell system.

Thus, the amount of gasifying agent in each Gibbs reactor is regulated, and as is the reaction equilibrium. The descriptions of the unit blocks in the combined system are summarized in Table 2.

Further, the produced SYNGAS is then employed as a thermal source of energy for the steam turbine system. The cold water stream (WATER) is first pressurized in the PUMP block before being supplied into the heat exchanger (HEX). The steam generated (W2) by the heat transfer is fed into the TURBINE, which generated power. The SYNGAS flow is cooled as a consequence of this process, and more power is obtained. Lastly, the CS5 component splitter block separates H_2 from other gas components before delivering H2DRY to the PEM fuel cell. Before being supplied to the PEM from the anode side (AIN), the H_2 is humidified in the B1 block. Compressed air is humidified and used as a feed to the cathode side (CIN) of the PEM in the B2 block. Excess H_2 was recirculated (H2REC) and mixed with the main feed in B8, while exhaust air COUT was cooled in B5 to recover demineralized water. The stream attributes for the

Table 2
Descriptions of the Aspen Plus unit blocks.

Block Name	Aspen Plus Unit Block Name	Description
R0	RYield	Converts non-conventional solid materials into conventional components.
R1 (400 °C) R2 (800 °C) R3 (1000 °C)	RGibbs RGibbs RGibbs	To simulate reactions between reactants and find probable products, the Gibbs energy minimization approach is utilized.
CS1	Sep	Canalizes the H_2O (100%), CO (100%) and CH_4 (55%) into the F4 stream.
CS2	Sep	Canalizes the C (100%) and ash (100%) into the F13 stream.
CS3	Sep	Canalizes the excess oxygen into the F12 stream.
CS4	Sep	Removes the undesired components (SO_x, H_2S, water, nitrogen, etc.).
CS5	Sep	Separates H_2 from COLDSYN for feeding into PEM fuel cell.
MIX B8	Mixer	Merges the inlet streams into a single output stream.
SPL1	FSplit	Splits the gasification agent in different ratios (20% ST1).
SPL2	FSplit	Splits the F7 for combustion process (17% F9).
CYCLONE	SSplit	Removes the solid particles from the gaseous stream.
HEX	HeatX	Uses the energy contrasts between cold and hot streams to transfer heat.
PUMP B4	Pump	Increases pressure of the fluid in the liquid phase to higher pressures.
TURBINE	Compr	Decreases pressure of the fluid in the vapor phase to lower pressures.
SEP	Flash2	At a given temperature and pressure, separates the liquid and vapor phases in equilibrium.
B1 B2	RadFrac	Models absorbers, strippers, etc. for 2 or 3-phase fractionation in single columns.
PEM	Custom Model	Unit block for PEM fuel cell calculations.
B5	Heater	Thermal and phase state changer to model heaters, coolers, condensers, etc.
SPLIT	SSplit	Divides feed based on splits specified for each substream.

proposed integrated system are listed in Table 3.

2.5. Artificial neural network modeling

Warren McCulloch and Walter Pitts invented a computer framework in 1943, laying the groundwork for neural networks, a future computing system [72]. ANN is a form of soft computing technology based on the human nervous system's functioning. ANN is comprised of artificial neurons, which are loads of single cells coupled to coefficients (or weight). The input layer of an ANN is an axon from a neuron, the hidden layer is dependent on model accuracy, and the output layer (output axon) provides the model's output result [73]. The input layer, which is the first layer, examines a signal as it enters the system. Following that, there are multiple hidden layers of neurons that cross the signal from the input level through the network with weighted linkages until it is outputted through the output level. The previous level provides input to every hidden neuron in the form of weighted signals [74]. The formula for an artificial neuron is as follows:

$$y_i = f\sum_{i=0}^{L}(x_i w_i + b) \tag{25}$$

where w_i is the weight for input x_i, and b denotes the bias. L defines the number of neurons, while y_i stands for the output of the model. Exception of input nodes, a nonlinear activation function (transfer function), represented as f, is used to describe a node's output. In this paper, the tangent sigmoid function was used as an activation function for hidden layers. It is defined as follows:

Table 3
Stream properties for the proposed CFB gasifier/steam turbine/PEM fuel cell plant.

Stream ID	Temperature (°C)	Pressure (bar)	Mass Flow Rate (kg/hr)	Heat Flow (kW)
COLDSYN	61.591	1.01325	1634.225	−2860.200
F1	25.000	1.01325	1000.000	−175.341
F2	400.000	1.01325	1200.000	−1781.450
F3	400.000	1.01325	816.676	−623.830
F4	400.000	1.01325	383.324	−1157.640
F5	800.000	1.01325	1616.676	−1511.150
F6	724.117	1.01325	2143.177	−2683.320
F7	724.117	1.01325	1969.973	−2677.390
F8	724.117	1.01325	1635.077	−2222.230
F9	724.117	1.01325	334.895	−455.156
F10	1050.000	1.01325	3908.100	−671.968
F11	1050.000	1.01325	807.434	−1591.790
F12	1050.000	1.01325	3100.700	919.874
F13	724.117	1.01325	173.203	−5.931
F14	1000.000	1.01325	143.176	−14.525
F15	724.117	1.01325	0.852	0.047
F16	61.591	1.01325	1551.446	−2985.480
H2DRY	61.591	1.01325	82.778	12.066
TBS	25.000	1.01325	1000.000	−406.443
OXYGEN	25.000	1.01325	3400.000	−0.246
SOLIDPRT	1000.000	1.01325	664.258	−1596.170
ST1	200.000	1.01325	200.000	−727.432
ST2	200.000	1.01325	800.000	−2909.730
STEAM	200.000	1.01325	1000.000	−3637.160
SYNGAS	724.117	1.01325	1634.225	−2222.280
W1	25.461	10.00000	800.000	−3562.460
W2	179.946	10.00000	800.000	−2924.540
W3	102.440	1.01325	800.000	−3006.760
WATER	25.000	1.01325	800.000	−3563.170
33	58.042	1.02000	57361.170	−252111.000
88	48.523	5.00000	57919.520	−255250.000
AIN	60.008	1.02000	381.033	−902.032
AIRFEED	63.000	5.00000	17824.440	185.137
AOUT	72.921	1.02000	125.343	−186.145
CIN	49.998	5.00000	18075.150	−815.060
COUT	78.714	5.00000	18330.830	−3430.420
GASOUT	63.000	1.01325	37.246	−56.239
H2FEED	62.150	1.01325	170.868	−120.956
H2O-1	60.000	1.50000	57571.330	−252892.000
H2O-2	50.000	5.00000	58170.230	−256250.000
H2OOUT-1	–	1.01325	–	–
H2OOUT-2	48.607	3.01325	642.466	−2831.330
H2REC	63.000	1.01325	88.096	−133.018
S33	25.000	1.01325	642.466	−2831.460
S7	63.000	1.01325	125.343	−189.257
S10	25.000	1.01325	17688.360	−1317.700

$$f(x) = \frac{e^{x} - e^{-x}}{e^{x} + e^{-x}} \tag{26}$$

3. Results

3.1. Model validation

Validation of the CFB gasifier and PEM fuel cell models must be performed before conducting the parametric analysis. Because an unreliable model cannot be evaluated, and correct conclusions cannot be considered. A comparison was done between the predicted gas composition produced during gasification from the proposed simulation model and the experimental results provided by Berrueco et al. [58] to validate the current model. The gasification process was modelled using inputs such as gasifier temperature, feedstock material characteristics, solid fuel and gasification agent flow rates, etc. in experimental study. As torrefied feedstock material, the researchers used Norwegian forest residues. They conducted a steam/air gasification procedure at 850 °C of gasifier temperature, 1 bar of gasifier pressure, 1.6 of steam to fuel ratio,

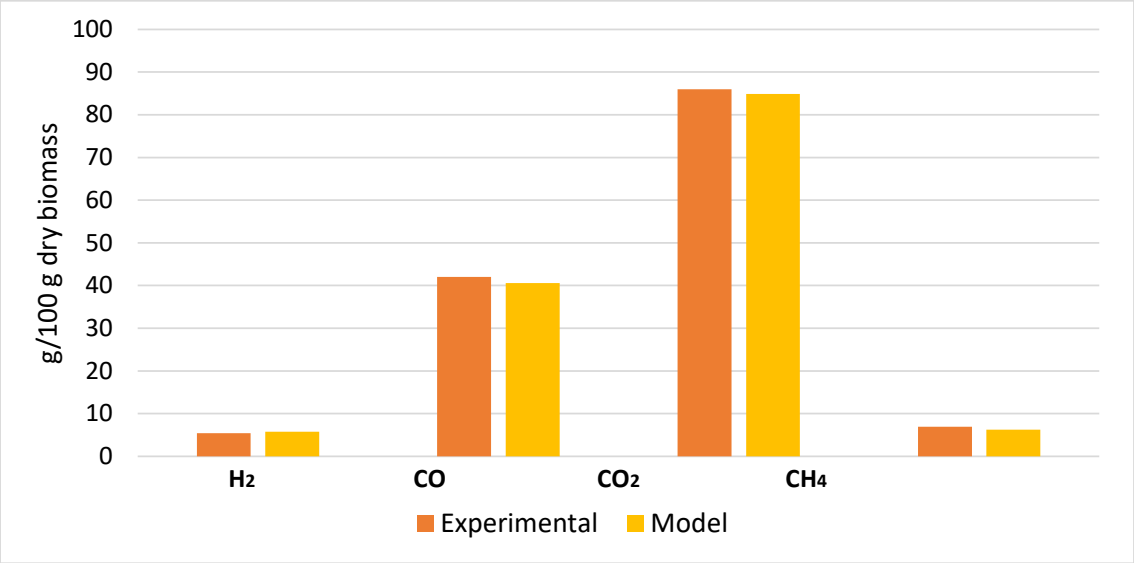

Fig. 3. Comparison of syngas composition between experimental result and CFB gasifier model result.

and 0.23 of equivalency ratio. As shown in Fig. 3, the syngas composition of CFB gasifier model is compared to the experimental result.

The current model demonstrates quite similar characteristics as the experimental results. Lower concentrations of gaseous products were predicted by the model than were seen in the experiments, except H_2. In thermodynamic equilibrium modeling, the conversion of hydrocarbons and methane makes estimating the methane gas concentration more challenging. The syngas composition also differs from experimental values owing to the CFB model's independence from design factors, disregard for reaction kinetics and fluid mechanics, and the reactor's infinite residence time. The syngas composition produced by the CFB gasifier model, on the other hand, did not significantly differ from the experimental data. Because the CFB gasifier model's auxiliary unit blocks (component splitters and stream splitters) were located between the reactors, providing to achieve an appropriate syngas composition. Therefore, the findings effectively approximate experimental studies when the CFB gasifier model is run with identical operating parameters and input variables. Parametric analyses can be carried out using the CFB gasifier model.

Validation of the PEM fuel cell model is also necessary in addition to the verification of the CFB gasifier model. The model was verified using data from a 70 kW PEM stack installation at AkzoNobel's chlor-alkali facility [75], where Nedstack PEM stacks of the identical type utilized in the proposed facility are being tested; and an industrial 1 MW PEM plant in Belgium from 2010 to 2015, developed by Nedstack and MTSA with a layout similar to the design of DEMCOPEM-2 MW plant [76]. Data from specific groups of stacks in the plant is compared to stack performance, resulting in power values within a 1% margin of error.

Table 4
Modeling findings and simulated stream conditions for the reference plant considered for model validation.

	Temperature (°C)	Flow rate (Nm^3/hr)
H_2 feed supplied to PEM (H2DRY)	50	1200
Recirculated H_2 stream (H2REC)	65	600
Air feed supplied to PEM (AIRFEED)	63	3450
Coolant stream (PEM inlet/outlet)	60/65	165
Water loop (Humidifiers inlet)	50	60
	Unit	**Value**
Gross DC electric power	kW	1040
Gross DC efficiency (H_2 LHV basis)	%	57.7
Recovered heat	kW	522
Consumption of auxiliaries	kW	67

Since field data is available for comparison, coolant flow and air humidification temperature are considered to be indicators of modeling thermal balancing precision. They have errors of less than 1.5% and 0.5%, which are similar to measurement uncertainties. The global mass balance is validated since the hydrogen inflow flow and air overflow are within the predicted nominal values. Table 4 lists the simulated 1 MW plant's stream data and overall performance.

The stacks are fed with humidified H_2 and air in quantities greater than the stoichiometric ratio (2.0 and 2.4 respectively). About 500 kW of heat is recovered from the fuel cells and supplied to the chlor-alkali plant. Fuel cells have a gross efficiency of approximately 60%. Auxiliary utilization is about 67 kW, with air and H_2 blowers taking up the majority of the capacity, followed by inverter systems and coolant pumps.

3.2. Parametric analysis

The effect of independent factors was assessed, and the dependent variables were investigated using the Aspen Plus process simulator's sensitivity analysis module. Gasifier temperature and pressure, and steam/fuel ratio were selected as independent factors that had a significant effect on the results. The rest of the parameters were maintained constant while one of them was changed in these parametric experiments. The temperature of the gasifier was adjusted between 600 and 1000 °C, the gasifier pressure was adjusted between 1 and 10 bar, and the steam/fuel ratio was varied between 0.5 and 1.5. Since operational variables have similar impacts on torrefied biomass samples, figures are only presented for the olive kernel sample to avoid bringing complexity to the plots. Changes depending on the sample's properties will be discussed in the following sections.

3.2.1. Effect of gasification temperature

The gasification process includes a significant number of complicated, homogeneous, and heterogeneous processes because it represents the thermal decomposition (partial oxidation) of solid fuels. Therefore, the temperature of the gasifier influences the direction of numerous endothermic and exothermic processes, resulting in changes in the concentrations of the produced components. According to Le Chatelier's principle, increasing the temperature favors endothermic reactions while changing the chemical equilibrium in exothermic reactions to the side of the reactants. High temperatures in the gasifier increase the concentrations of H_2 and CO while decrease the

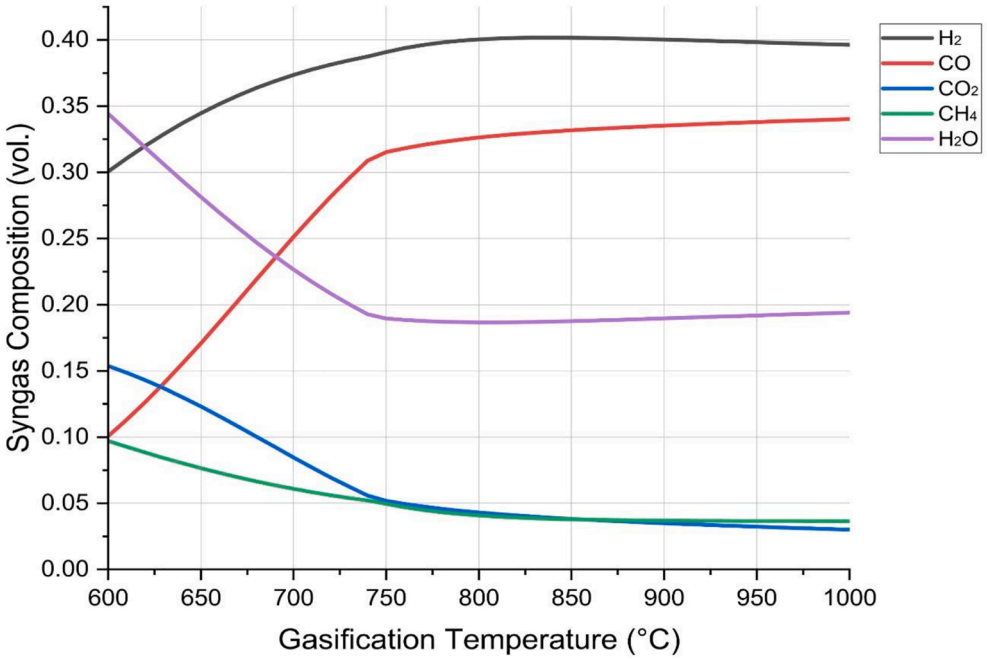

Fig. 4. Effect of gasification temperature on syngas composition.

concentrations of CO_2 and H_2O. Possible explanations for the change in gaseous component percentages can be explained by the Boudouard reaction and the water–gas reaction. Moreover, when the temperature increases, the amount of CH_4 in the syngas decreases dramatically. The forward process of steam-methane reforming at high temperatures causes the degradation of CH_4. The effect of gasification temperature on syngas composition is shown in Fig. 4.

The graph demonstrates that while H_2 and CO concentrations in the syngas increase at high temperatures, CH_4, H_2O, and CO_2 concentrations reduce. The H_2 concentration increased from 30.06% to 39.62%, and the CO concentration increased from 10.08% to 34.02%. In addition, the CO_2 concentration decreased from 15.37% to 3.00%, the H_2O concentration decreased from 34.42% to 19.40%, and the CH_4 concentration decreased from 9.70% to 3.65%. The other torrefied biomass samples showed similar trends in shifting gas component concentrations. The rise in H_2 concentration at high temperatures can be explained by the increased rate of steam-methane reforming reaction and the accelerating forward reaction of the water–gas, which is an endothermic reaction in

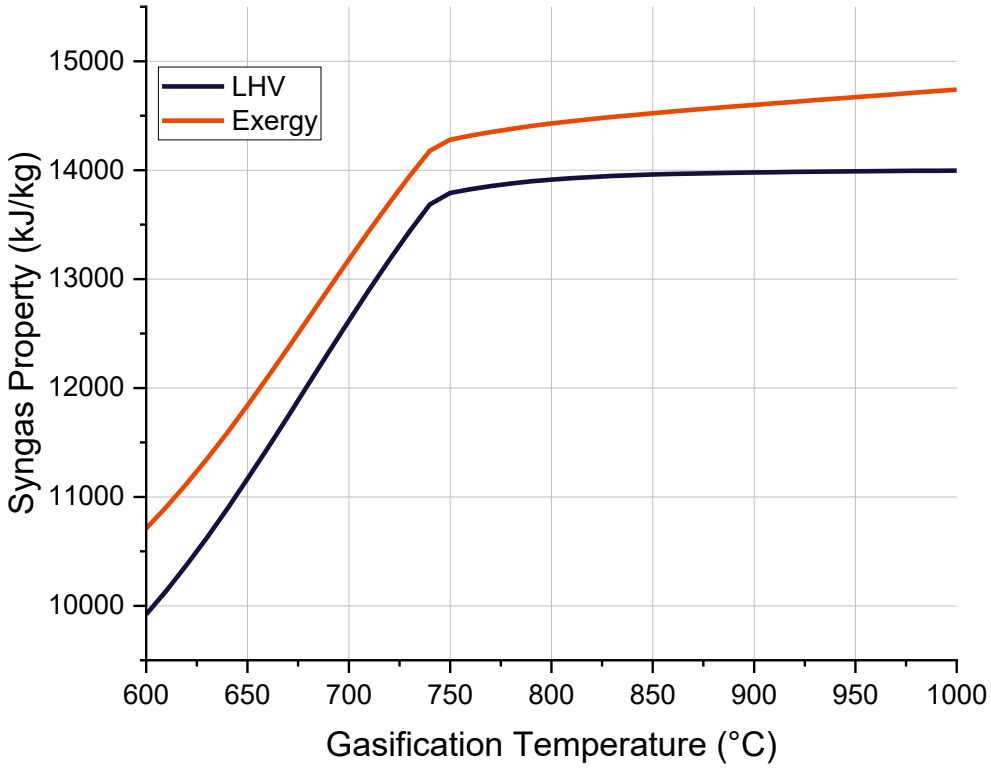

Fig. 5. Effect of gasification temperature on syngas LHV and exergy.

the solid–gas phase. Moreover, the molar concentration of H_2 rises at first, then begins to decrease. The highest fraction of the H_2 component was reported at 840 °C. Other researchers have also reported on fluctuating behavior of H_2 [77,78]. Higher temperatures suppress methanation and water–gas shift processes, both of which are exothermic and result in the production of syngas with lower H_2 concentrations. The variation in H_2 could be due to the combined effects of processes in the gasifier [79]. The fluctuation in H_2 concentration, according to Vikram et al. [80], is caused by the major processes, which are the water–gas shift and char reforming reactions. Exothermic water–gas shift reactions shift backward at high temperatures, following Le Chatelier's principle, resulting in the formation of the reactants CO and H_2O. A negative correlation was also found between CO and CO_2 components as the gasifier temperature is raised. At elevated temperatures, the Boudouard reaction, which is an endothermic process, is shifted forward, which could explain the change. Furthermore, up to 740 °C, the olive kernel sample revealed a dramatic rise in CO fraction and reduction in CO_2 fraction, although the change is slower at higher temperatures. As aforementioned, the temperature value varies depending on the torrefied biomass feature, but the behavior is consistent. Additionally, the concentration of CH_4 reduces as the temperature rises. The forward process of steam-methane reforming accelerates at high temperatures, leading in CH_4 degradation. The composition of the syngas, which changes with temperature, has an impact on its heating value. Fig. 5 shows the effect of gasifier temperature on syngas LHV and exergy.

A continual increase was observed in syngas LHV between 600 and 1000 °C. For the olive kernel sample, syngas LHV increased from 9920.60 kJ/kg to 13995.99 kJ/kg. Since the H_2 and CO concentrations increased with temperature, the LHV was enhanced despite the decrease in CH_4 concentration. The reduction in H_2O and CO_2 concentrations due to the increase in gasification temperature enhanced the syngas LHV as well. In addition, syngas LHV increase is strong up to a certain gasification temperature, but it slows down as the temperature rises. Above 750 °C, the LHV growth has slowed. This can be explained by the fact that the syngas composition has not varied considerably above 750 °C. Since the CO fraction curve and the LHV curve are so equivalent, it can be concluded that syngas CO content has a major impact on LHV. When operated at high temperatures, the gasifier produces hot gas products with a considerable work capacity, resulting in an increase in physical exergy. Also, when the temperature increases, the composition of the syngas changes, having an influence on the chemical exergy. A steady increase in syngas exergy was observed between 600 and 1000 °C, similar to the syngas LHV. The syngas exergy for the olive kernel sample increased from 10710.57 kJ/kg to 14739.51 kJ/kg. The increment in exergy slows beyond a certain temperature (approximately 750 °C), identical to the syngas LHV profile. This is because the change in syngas composition is less at higher temperatures than at lower temperatures. Unlike the rise in LHV, however, the increase in exergy does not slow down much since syngas work capacity improves with increasing temperature despite the less changing composition.

3.2.2. *Effect of gasification pressure*

Gasifier pressure, likewise gasifier temperature, is a vital operational variable that has a significant influence on the performance of the gasification process. The gasifier pressure has a considerable impact on the gasification processes' equilibrium states. According to Le Chatelier's principle, a change in pressure shifts an equilibrium state to the reaction side, where there are less moles of gas. Due to the steam-methane reforming and hydrogasification processes, raising the gasifier pressure had a favorable effect on the CH_4 concentration since the equilibrium states shifted to the side of lower moles of gas. At higher pressures, the hydrogasification, reverse water–gas, and reverse steam-methane reforming processes also lower the H_2 concentration. Pressure changes have no influence on the water–gas shift reaction, which has no effect on the H_2 fraction change. Furthermore, the Boudouard reaction raised the mole fraction of CO_2 while decreasing the mole fraction of CO when the gasifier pressure was increased. Moreover, the reduction in CO content due by greater gasifier pressure can be explained by reverse steam-methane reforming, partial combustion, and water–gas reactions. Fig. 6 demonstrates the effect of gasification pressure on syngas composition.

Higher gasification pressures enhanced H_2O, CH_4, and CO_2 concentrations while decreasing CO and H_2 concentrations, as seen in the Fig. 6. For the gasification of torrefied olive kernel sample, the H_2

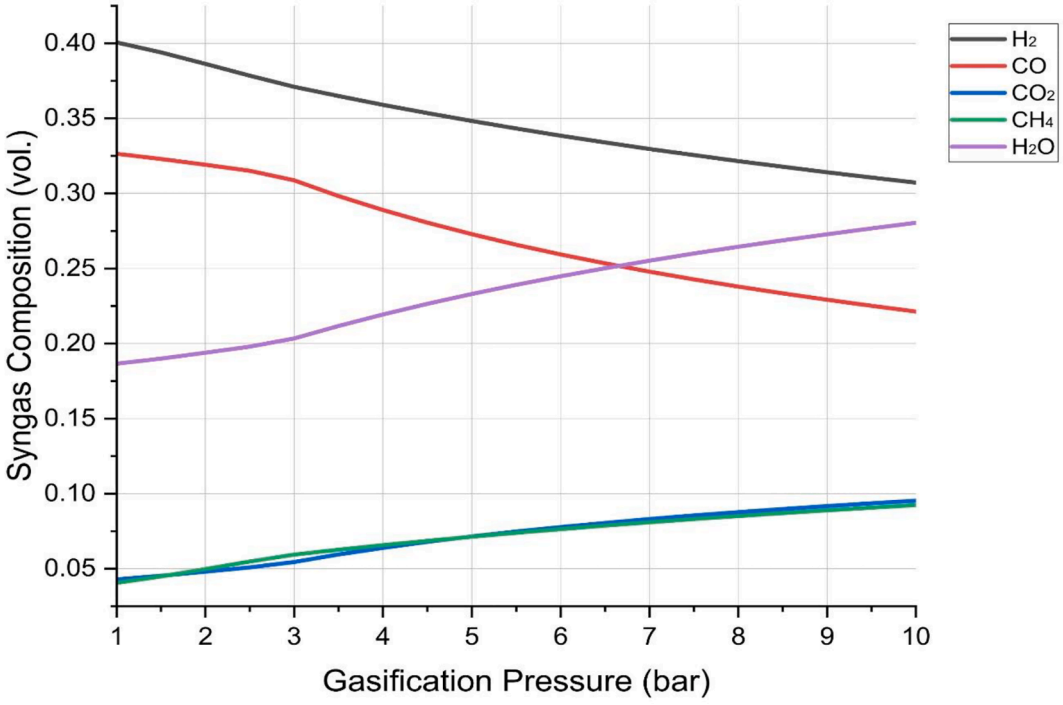

Fig. 6. Effect of gasifier pressure on syngas composition.

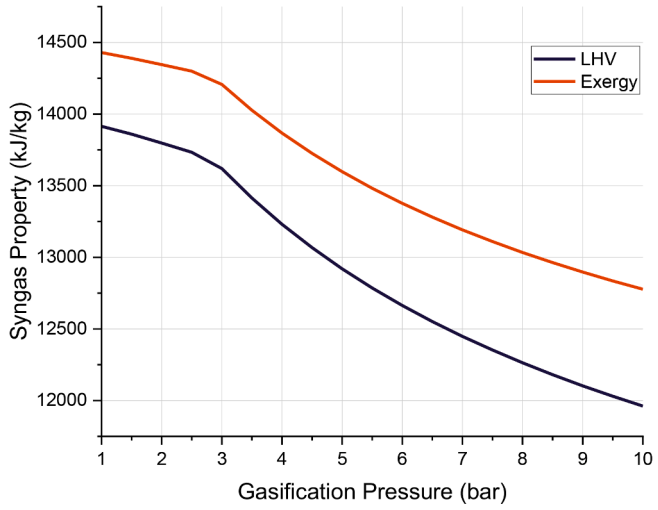

Fig. 7. Effect of gasifier pressure on syngas LHV and exergy.

concentration decreased from 40.05% to 30.72% and CO concentration decreased from 32.63% to 22.13%. Further, CH_4 concentration increased from 4.06% to 9.23%, H_2O concentration increased from 18.66% to 28.04% and CO_2 concentration increased from 4.29% to 9.53%. Although an increase in gasification pressure results in a continual reduction in the favorable gas concentration, the quality of the syngas can be considered to decline more rapidly at higher pressures, particularly over 3 bar. Briefly, increasing gasification pressure only increased the proportion of CH_4 among the favorable gases. The effect of gasification pressure on syngas LHV and exergy is depicted in Fig. 7.

As seen in Fig. 7, gasification at high pressures reduced the thermal value of the syngas obtained. For torrefied olive kernel sample, syngas LHV decreased from 13914.52 kJ/kg to 11961.49 kJ/kg. The syngas LHV decline was more substantial in gasification operations above 3 bar pressure, just as it was with the change in syngas composition (Fig. 6). Syngas exergy exhibited a very similar behavior to syngas LHV change when the relationship between syngas exergy and gasifier pressure was examined. For torrefied olive kernel sample, syngas exergy decreased from 14429.02 kJ/kg to 12776.99 kJ/kg. Beyond 3 bar pressure, syngas exergy diminishes more dramatically in gasification operations. Further, the syngas exergy is solely impacted by the syngas composition since the gasifier temperature remains constant during the parametric run. However, unlike syngas LHV, syngas exergy includes the exergy value of non-combustible components in the calculation, resulting in a larger syngas exergy value than syngas LHV under the same operating conditions.

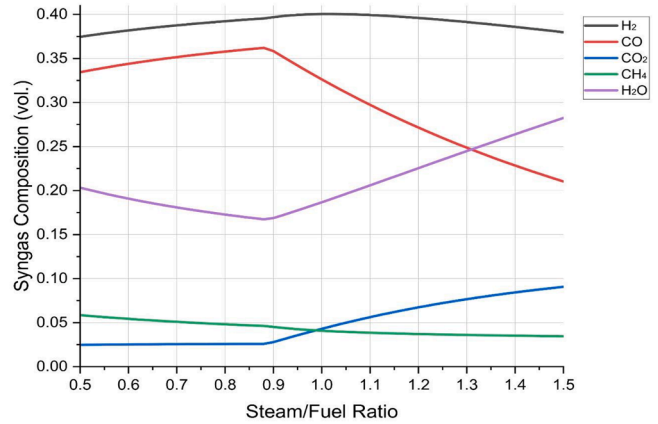

Fig. 8. Effect of steam/fuel ratio on syngas composition.

3.2.3. *Effect of steam/fuel ratio*

The ratio of steam entering the reactor to the fuel supplied to it is described as the steam/fuel ratio. Determining the proper steam/fuel ratio depending on the operating conditions is critical in real-world applications. The partial pressure increases as the amount of steam in the reactor increases, boosting various homogeneous and heterogeneous reactions. Nonetheless, the temperature of the gasifier drops, and the cost of steam production is not negligible. The concentration of H_2 in the syngas improves as the steam/fuel ratio increases due to heterogeneous char-steam gasification processes, and this has been observed for a number of solid fuels [81,82]. Moreover, when H_2O levels are high, the water–gas shift reaction shifts to the products side, resulting in a higher proportion of H_2 and CO_2. The steam-methane reforming forward process enhances CH_4 degradation even further with continuous H_2O feeding. Fig. 8 demonstrates the effect of steam/fuel ratio on syngas composition.

The H_2 concentration increased until steam/fuel ratio was 1.02 from 37.46% to 40.04%, and then decreased to 37.97% beyond that steam/fuel ratio. Likewise, the CO concentration reached its maximum (36.20%) at the steam/fuel ratio of 0.88, and its concentration decreased beyond this steam/fuel ratio. The H_2O and CO_2 concentrations increased dramatically beyond the steam/fuel ratio of 0.88. It should be noted that the H_2O supply was excessive beyond this steam/fuel ratio. Similar behavior in the change of gas component concentrations can be seen for the other torrefied biomass samples, on the other hand, optimum steam/fuel ratio can change depending on the properties of the solid material. The composition of the syngas, which changes with the steam/fuel ratio, has an impact on its calorific value. Fig. 9 illustrates the effect of the steam/fuel ratio on syngas LHV and exergy.

The continuous supply of steam to the gasifier caused a decline in syngas LHV owing to excessive H_2O concentrations and an increase in CO_2 concentration, as illustrated in Fig. 9. Syngas LHV decreased from 14562.94 kJ/kg to 10941.32 kJ/kg for the torrefied olive kernel sample. However, the syngas LHV increased until the steam/fuel ratio reached 0.88 (from 14562.94 kJ/kg to 14765.65 kJ/kg), after which the syngas calorific value started to decline. According to the other researchers [38,83], when the concentration of combustible gas components in the syngas diminished with increasing H_2O concentration, the heating value of the syngas decreases. Changes in syngas composition and thermal value also had an effect on the exergy value. Since the syngas exergy value was primarily influenced by the chemical composition, while the gasifier temperature remained constant, the syngas exergy change was approximately equal to the syngas LHV change. Syngas exergy increased from 15108.66 kJ/kg to 15230.31 kJ/kg in the torrefied olive kernel

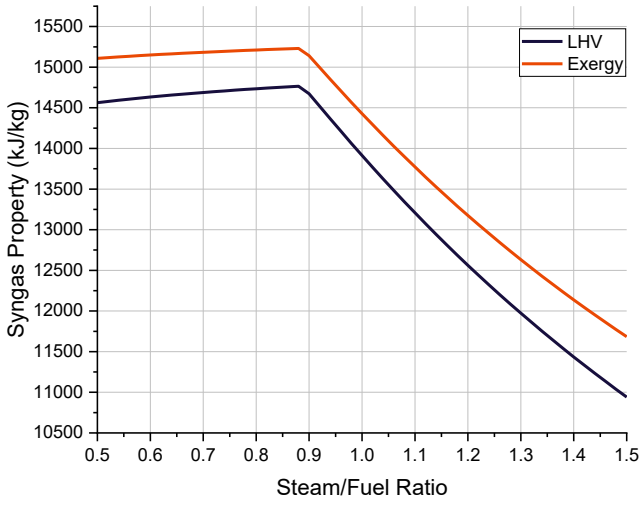

Fig. 9. Effect of steam/fuel ratio on syngas LHV and exergy.

gasification process up to a steam/fuel ratio of 0.88, then declined to 11683.66 kJ/kg. LHV represents the available thermal energy that can be obtained when syngas is burned. As a consequence, the CO_2 and H_2O components of the syngas cannot be regarded to contribute to the LHV. On the other hand, each component of syngas contributes to the total exergy value. Therefore, the syngas exergy value was determined to be greater than the syngas LHV under identical conditions.

3.2.4. *Effect of operating parameters on H_2 production*

The influence of gasification operation variables on syngas properties has been studied in previous parametric research. The operating conditions necessary for syngas production with the appropriate composition and heating value were discovered in these investigations, which were discussed on the olive kernel sample. Also, PEM integration is an essential application in the model provided in this paper, and hydrogen is the source of fuel cells. Therefore, determining the quantity of H_2 produced as well as the concentration of H_2 in the syngas is crucial. Each fuel cell is constructed to provide a certain range of power, and

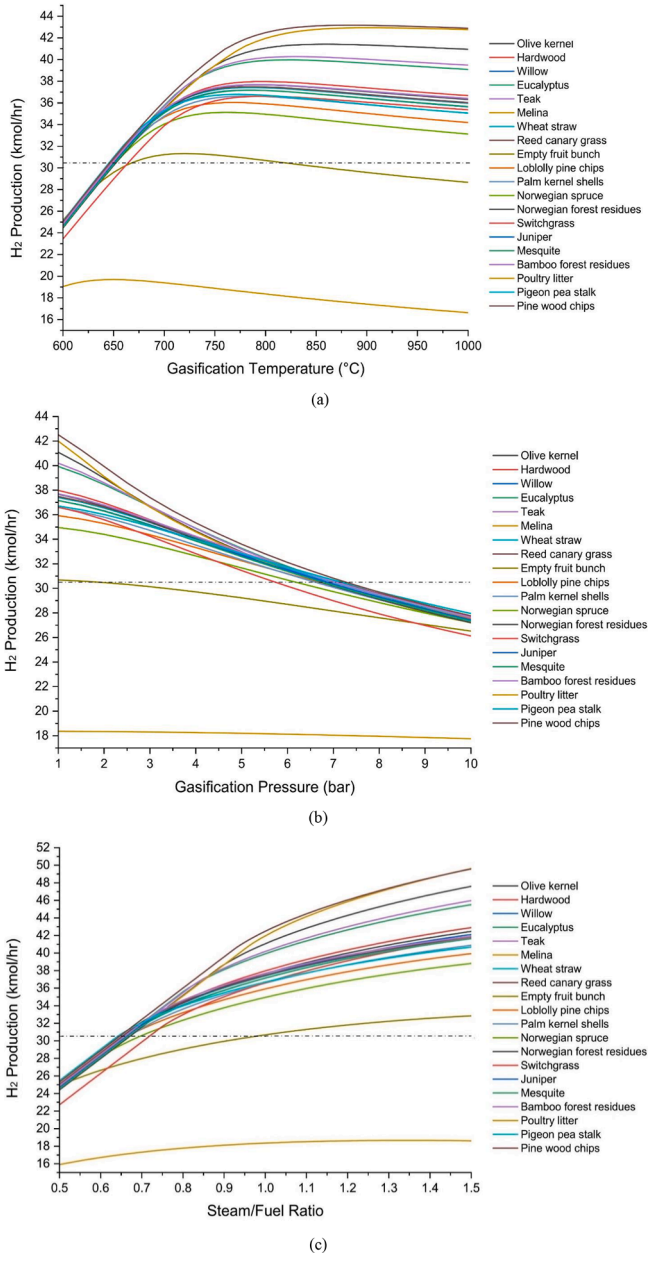

Fig. 10. Effect of operating parameters on H_2 production.

design factors/constraints mandate specific operating conditions (operating temperature and pressure, H_2 supply etc.). The minimum amount of H_2 to be fed was determined to be approximately 30.5 kmol/hr in the sensitivity analysis conducted for the PEM fuel cell model, the details of which were discussed in Section 2.3. Hence, sensitivity analysis was performed for each fuel in this part to identify the minimal operating parameters particular to each torrefied biomass sample, and indirectly preliminary research was conducted to produce an accurate data set for neural network training. Fig. 10 illustrates the effect of operational conditions on H_2 production.

Operational circumstances must satisfy certain necessary criteria regardless of fuel in order to operate a PEM fuel cell combined with a CFB gasifier. These minimal requirements, however, largely depend on the fuel's qualities. A dashed line parallel to the x-axis was drawn from the point of 30.5 kmol/hr H_2 production to make identifying these conditions easier. When the temperature of the gasifier was examined, it was observed that an operating temperature of less than 650 °C, on average, could not provide the requisite minimum H_2 production. This can be explained by the fact that endothermic reactions like water–gas and steam-methane reforming, which are essential for H_2 production, necessitate high temperatures. Another endothermic process, the Boudouard, enhances CO production at high temperatures. Despite being exothermic, the water–gas shift process can have enhanced H_2 production owing to the the amounts of CO produced. Furthermore, at any gasifier temperature, the torrefied poultry litter sample cannot be used for PEM integration. The torrefied empty fruit bunch sample can be used only at temperatures of 675 °C − 825 °C. When compared to other torrefied samples, the torrefied poultry litter sample had the greatest ash value and the lowest C concentration. In addition, the O/C and H/C values of poultry litter and empty fruit bunch samples are higher than those of other samples. These features, which are indicative of poor solid fuel quality, make using torrefied poultry litter and torrefied empty fruit bunch samples as fuel in a PEM integrated CFB gasifier system impossible or problematic. Pine wood chips and melina samples, on the other hand, were found to be the torrefied biomass samples that yielded the most H_2 at the identical gasification temperature. In comparison to other samples, both torrefied samples contain low ash and high C content, as well as low O/C and H/C ratios.

Gasification at high pressures decreases H_2 synthesis, as stated in Section 3.2.2. Gasification pressures more than 6.5 bar on average are not viable for the PEM integrated CFB gasifier model (Fig. 10b), according to this finding. At any operating pressure, a sample of torrefied poultry litter does not produce the minimum essential H_2. Torrefied empty fruit bunch sample can also provide the required H_2 only in a narrow gasifier pressure range (<2 bar), similar to what was observed at gasifier temperature. Solid fuels with high O/C and H/C ratios necessitate operating the PEM integrated CFB gasifier at low pressures. In comparison to other biomasses, torrefied melina and torrefied pine wood chips samples produced larger quantities of H_2 at the same operating pressure. As a result, it's important to note that in PEM integrated gasifier systems, high-quality solid fuels can tolerate operating at relatively high pressures.

As previously indicated, increasing the quantity of steam given to the reactor accelerates the forward shift of reactions including steam-methane reforming, water–gas, and water–gas shift, resulting in more H_2 production. However, as demonstrated in Fig. 10c, gasification processes with steam/fuel ratios less than 0.65 averagely were unable to provide the essential H_2. While any quantity of steam feed is not enough for the torrefied poultry litter sample, at least 1.0 steam/fuel ratio is necessary for the torrefied empty fruit bunch sample. Torrefied melina and torrefied pine wood chips samples offer larger quantities of H_2 at the same steam/fuel ratio, as seen in other operational conditions. The common factor within all three graphs was that solid fuels with high H/C and O/C ratios are less impacted by operational variable change. Especially, the gasifier pressure and the steam/fuel ratio had a little impact on the torrefied poultry litter sample. This is because fuels with

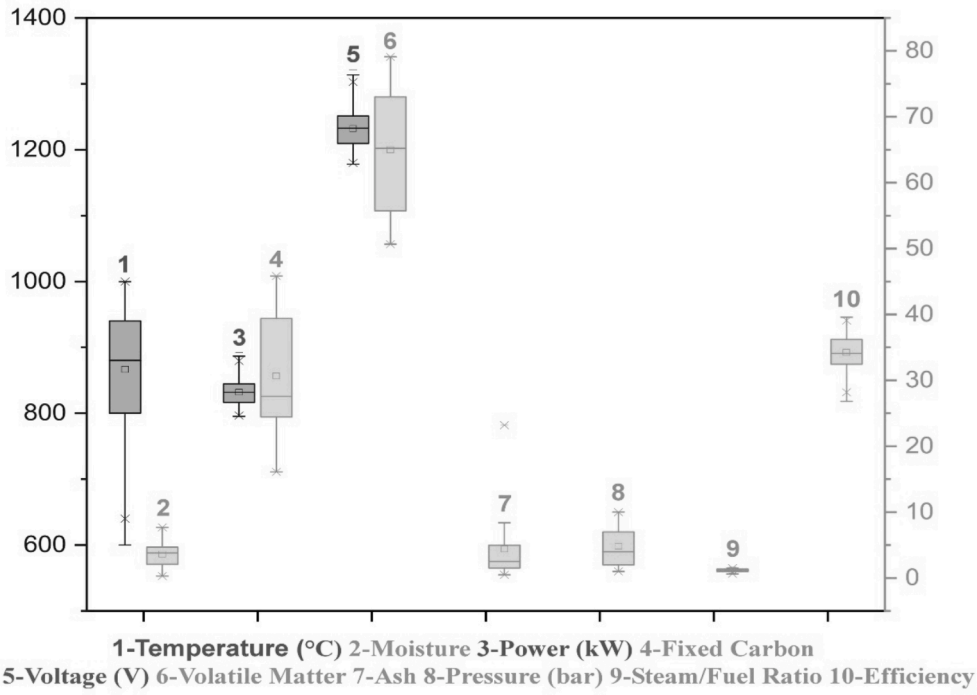

Fig. 11. The boxplot diagram of input and output variables.

less reactive structures yield less amount of gaseous components.

3.3. Creation and analysis of the dataset

The influence of the gasifier's operating parameters on the syngas characteristic was addressed in the parametric analysis section (Section 3.2). As this research comprised the integrated PEM fuel cell system, the impact of the same operating parameters on H_2 production was investigated next. As a consequence, it was decided which sections of the overall data generated as a result of parametric analysis must be discarded. For 20 different torrefied biomass samples, parametric analysis included a temperature increase of 10 °C, a pressure increase of 0.5 bar, and a steam/fuel ratio increase of 0.01. Thus, a dataset with a total of 172,220 rows was constructed. A set of 77,609 lines was obtained after operating conditions that would not be suitable for the PEM fuel cell were eliminated (operational parameters with less than 30.5 kmol/hr H_2 production). Fig. 11 shows the boxplot diagram of the parameters preferred as input and output variables in this study.

Using proximate analysis data (db.%) of torrefied biomass sample and gasification operational conditions, PEM power, voltage, and efficiency (LHV based) are estimated in this research. The y-axis on the left is used to follow variables in black color, while the y-axis on the right is used to follow variables in grey color. When the variables of the gasifier operational conditions were evaluated, high gasification temperatures and steam/fuel ratios were found to be the most common. In the dataset, the average gasifier temperature was determined to be 866.70 °C, and the average steam/fuel ratio was calculated to be 1.16. Despite the fact that parametric studies have depicted that low gasification temperatures limit H_2 production, gasification temperature of 600 °C have been taking place in the dataset. This demonstrates that CFB gasification process can supply the needed quantity of H_2 at high steam/fuel and low gasifier pressures at lower temperatures. However, the dataset's lowest steam/fuel ratio was determined to be 0.6. This demonstrates that under any operating environment, none of the torrefied biomass materials utilized in this research can deliver the needed H_2 at a steam/fuel ratio of less than 0.6. When the gasifier pressure was analyzed, it was determined that the dataset had a minimum of 1 bar and a maximum of 10 bar, with an average pressure of 4.82 bar. However, 75% of the pressure data in the dataset was up to 7 bar, which is consistent with the observation that most torrefied materials do not produce enough H_2 at pressures more than 6.5 bar (Fig. 10b). When the attributes of the torrefied samples were investigated, the moisture data showed that the lowest and highest values were 0.30 and 7.68, respectively. The average moisture value was found to be 3.61. Moreover, the mean values for fixed carbon and volatile matter were observed to be 30.65 and 64.96, respectively. The minimum and maximum values of the variables moisture, fixed carbon, and volatile matter reveal that the dataset includes the outcomes of all torrefied materials. However, the dataset's highest ash value (23.20) indicates that the outputs of the poultry litter sample are not included. This conclusion is in line with Section 3.2.4's findings. In addition, the average ash value in the dataset is 4.38. The PEM power was estimated to be between 795.26 kW and 891.86 kW when the distribution of output variables was examined. With a standard deviation of 19.77 kW, the average power was 831.74 kW. Also, the average voltage was 1232.21 V with the maximum and the minimum values of 1178.17 V and 1321.27 V, respectively. LHV-based PEM efficiency, the last output variable, was found to be between 26.82% and 39.58%. PEM efficiency was determined to be 34.22% on average, with a standard deviation of 2.64%. The PEM fuel cell is designed to function at greater capacities and efficiency in practice. However, variables such as power, voltage, and efficiency were discovered in this range when considering aspects such as the proposed CFB gasifier model's capacity, H_2 productivity, the operating conditions evaluated, and the physicochemical attributes of the torrefied solid fuels used. Fig. 12 shows the impact of the characteristics of torrefied biomass samples used for this work on output metrics such as PEM power, voltage, and efficiency.

The x-axis is fixed carbon (FC), y-axis is volatile matter (VM), z-axis is ash, and height axis is output variables for the plots (Fig. 12a, b and c) covering proximate analysis results. On the other hand, the x-axis is carbon (C), y-axis is hydrogen (H), z-axis is oxygen (O), and height axis is output variables for the plots (Fig. 12d, e and f) containing ultimate analysis results. Power and voltage variables are similarly impacted by input parameters when the effects of both ultimate and proximate analysis findings on output variables are investigated. This can be

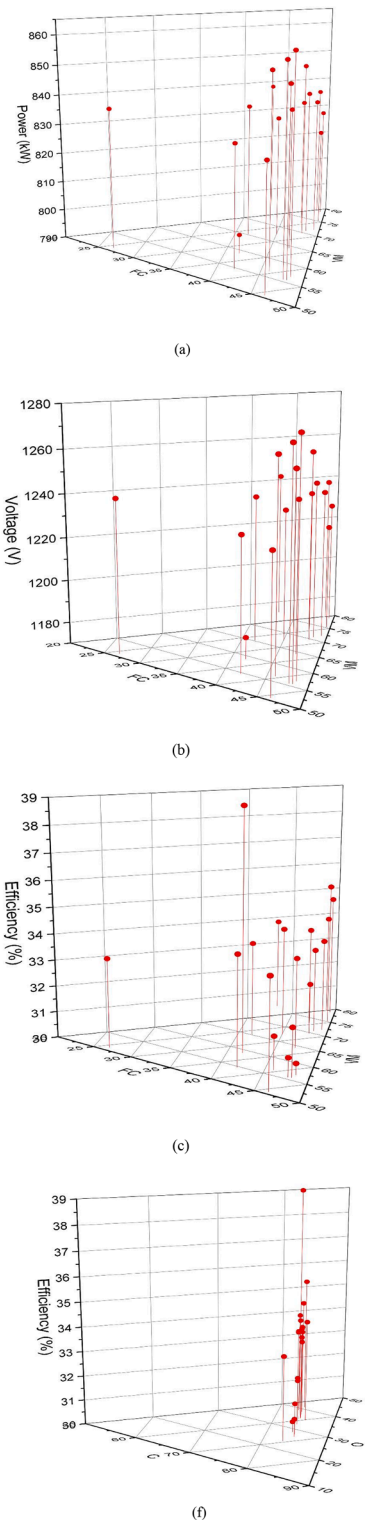

Fig. 12. The effect of proximate and ultimate analysis results of torrefied biomass samples on PEM power, voltage and efficiency (temperature: 800 °C, steam/fuel ratio:1.0, and pressure:1 bar).

explained by the fact that the power and voltage parameters are directly proportional. However, the results of proximate analysis do not have a linear relationship with the power and voltage. Pine wood chips, melina, and olive kernel are the torrefied samples with the highest power and voltage output, with fixed carbon values of 41.72%, 42.19%, and 39.37%, respectively. These values are greater than the dataset's average fixed carbon value of 30.65%, but the empty fruit bunch sample, which produces the minimum power and voltage, also has a fixed carbon ratio of 32.65%. Additionally, fixed carbon ratios of 37.27% and 45.82% are found in palm kernel shells and pigeon pea stalk samples respectively, and these torrefied materials provide the lowest fourth and sixth power and voltage, respectively. When considering the impact of volatile matter percentage on power and voltage outputs, it's important to note that large concentrations reduce power and voltage output. It should be also noted that the three samples that provide the greatest power and voltage output had an average volatile matter content of approximately 56%, which is lower than the dataset's average (64.96%). However, since the empty fruit bunch, the sample with the lowest power and voltage output, had a volatile matter concentration of 59.03%, it's difficult to establish concrete conclusions. The ash content in the torrefied material, like the fixed carbon and volatile matter results, does not have a linear effect on the power and voltage output. Since torrefied materials often contain low amounts of ash, their influence on output could be minor. Further, when the impact of the ultimate analysis findings on power and voltage outputs is investigated, a more distinct pattern is observed. Increased power and voltage outputs are highly dependent on high carbon content and low oxygen concentration. Pine wood chips, melina, and olive kernel samples, which are the torrefied samples that produce the maximum power and voltage output, have an elemental carbon component of above 60%. Furthermore, the proportion of elemental oxygen in the same three samples is less than 27%. These fraction values are beyond and below at the average values. However, since the distribution changes depending on the type of torrefied material, it's difficult to mention about a strong relation between elemental carbon and oxygen concentration with power and voltage. Similarly, since the elemental hydrogen concentration does not change considerably depending on the type of torrefied material, the hydrogen concentration cannot be considered to have a linear relationship with the power and voltage output. On the contrary, the power and voltage variations stated so far, which are dependent on the fuel characteristic, have a detrimental effect on PEM efficiency. PEM efficiency is improved by low elemental carbon and high elemental oxygen concentration, as well as low fixed carbon and high volatile matter. However, identifying a consistent pattern is challenging. Rather of focusing on the influence of elemental carbon, hydrogen, and oxygen concentrations in the solid material on the output variables, examining the effect of the H/C and O/C ratios on the output variables, as in the Van Krevelen diagram, can be more informative. Fig. 13 visualizes the effect of H/C and O/C ratios of torrefied materials on output variables.

The influence of elemental carbon, oxygen, and hydrogen ratios on PEM outputs behaved more systematically, as predicted. Despite the fact that there are fluctuations, a generalized pattern can be seen. In addition, variations in the H/C and O/C ratios had a comparable effect on power and voltage outputs, as anticipated, whereas efficiency was influenced in the opposite manner. Torrefied materials with lower H/C and O/C ratios improve power and voltage output, as shown in plots. The fact that the solid fuel is positioned in the Van Krevelen diagram's peat and lignite zones, i.e., as the carbonization degree increases, improves the power and voltage. Solid fuels having a high H/C and O/C ratio, such as torrefied materials in the biomass zone of the Van Krevelen diagram, on the contrary, improved PEM efficiency. To conclude, as the degree of carbonization of the solid material grows, the power and voltage increase, but the efficiency diminishes. To summarize the impact of fuel properties on PEM outputs, ultimate analysis parameters were more reliable indicators than proximate analysis parameters. Furthermore, H/C and O/C ratios, rather than elemental carbon, hydrogen, and oxygen concentrations, were more useful metrics for PEM outputs. Nonetheless, one of the input factors used to predict PEM outputs in this paper is the proximate analysis results of the torrefied biomass sample. This is for several reasons: first, it makes the problem more challenging. Second, the torrefied materials' proximate analysis results are not in the extreme range, i.e., they are consistent with the overall biomass/

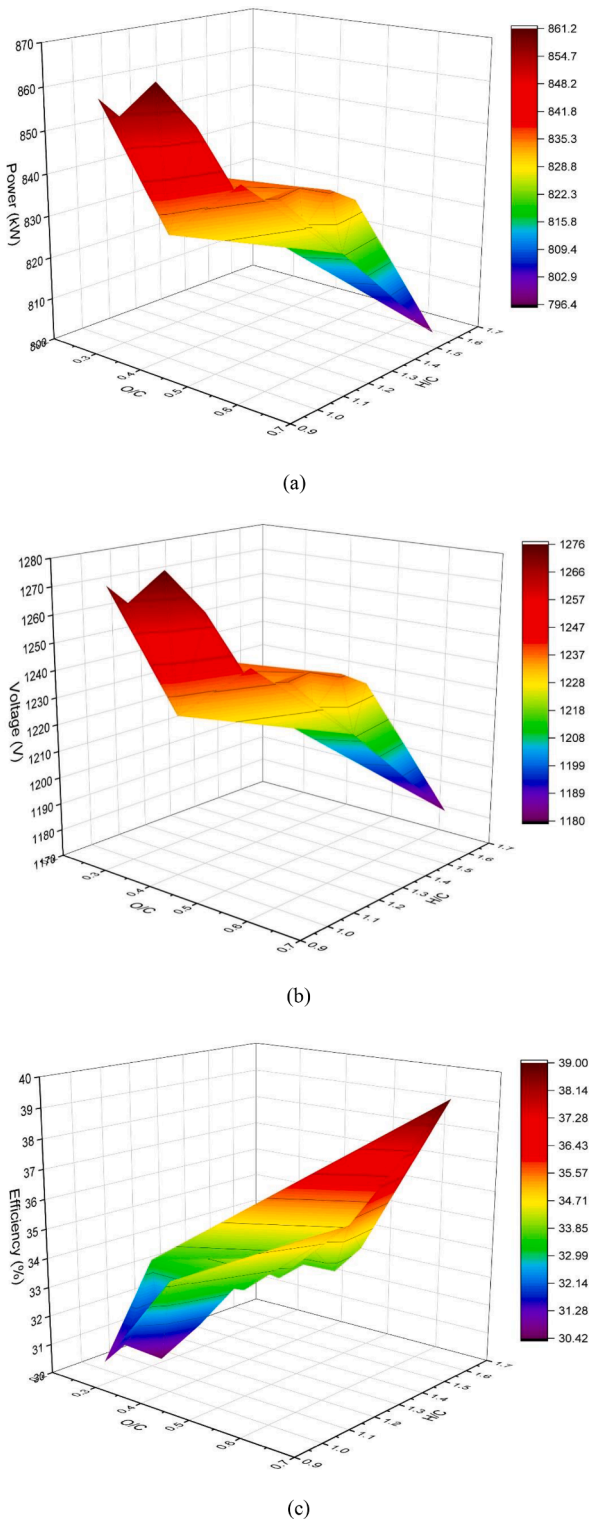

Fig. 13. The effect of H/C and O/C ratios of torrefied materials on PEM power, voltage and efficiency (temperature: 800 °C, steam/fuel ratio:1.0, and pressure:1 bar).

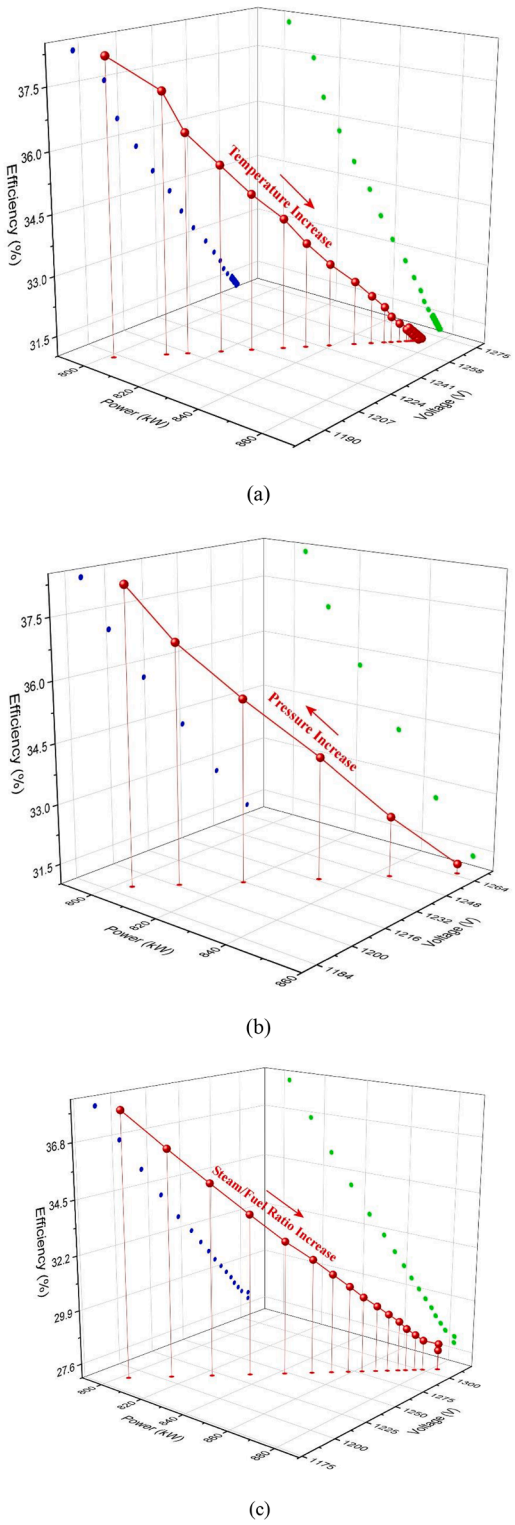

Fig. 14. The effect of gasifier operating conditions on PEM power, voltage and efficiency.

torrefied biomass physicochemical characteristic. Finally and most importantly, proximate analysis findings can be obtained using basic procedures and ordinary equipment, but ultimate analysis requires difficult methods and specific instruments [84]. In addition to the fuel characteristic, the effect of CFB gasifier operational conditions on PEM power, voltage and efficiency is illustrated in Fig. 14 for the olive kernel sample.

For the torrefied olive kernel sample, the gasifier temperature is between 660 °C and 1000 °C (an interval of 10 °C), the gasifier pressure is between 1 bar and 6 bar (an interval of 1 bar), and the steam/fuel ratio is between 0.7 and 1.5. (an interval of 0.05). In fact, conclusions identical to those stated for Fig. 10 can be inferred from the behaviors in Fig. 14. High gasification temperatures and steam/fuel ratios resulted in

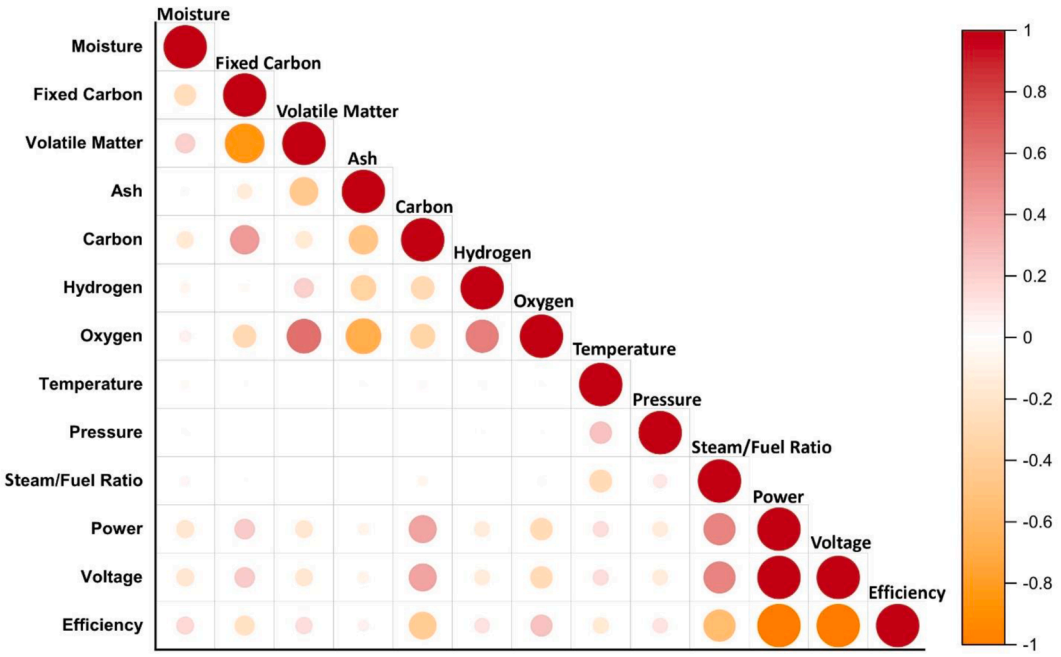

Fig. 15. The correlation map for selected parameters.

higher power and voltage outputs while decreasing efficiency. Higher gasification pressures, on the other hand, lowered power and voltage outputs while increasing efficiency. This is a straightforward deduction from the relationship between operational conditions and H_2 production. High gasification temperatures and steam/fuel ratios enhanced H_2 synthesis, but high gasification pressure reduced production. When a result, as the amount of H_2 delivered to the PEM fuel cell model rises, the power and voltage outputs increase but the efficiency decreases. Increasing the temperature of the gasifier and the steam/fuel ratio does not result in the same rise or reduction in output variables. H_2 synthesis slows and even begins to decline at higher temperatures and steam/fuel ratios. On the other hand, since the gasifier's continually increasing pressure significantly limits H_2 production, it has a comparable impact on PEM outputs.

The correlations between output variables (power, voltage, and efficiency), input variables (moisture, fixed carbon, volatile matter, ash, gasifier temperature, gasifier pressure, and steam/fuel ratio), and other fuel properties (carbon, oxygen, and hydrogen) can be identified and the scientific rationale for them can be discussed. Fig. 15 depicts the correlations between the factors stated above, using the correlation matrix as a tool.

Colors show whether there is a positive or negative relationship between the parameters in the correlation matrix, and the intensity of the color and the size of the circle indicate the strength of the relationship. At first inspection, the correlation matrix's weak negative or weak positive coefficients stand out. However, a variety of other correlation coefficients are also observed. Except for output variables, the correlation coefficient between operating parameters and other

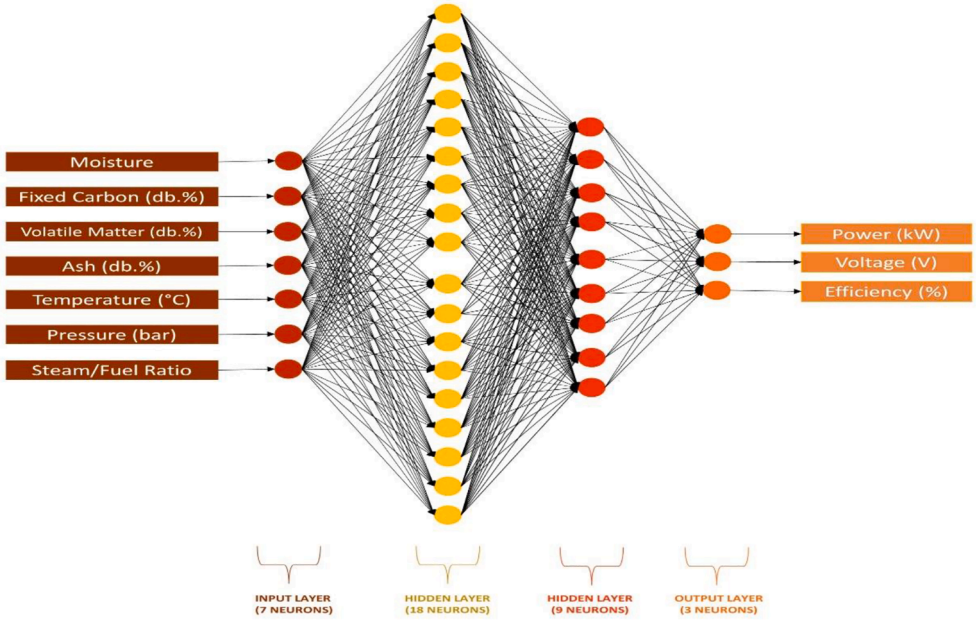

Fig. 16. The structure of the ANN developed in this study.

variables is close to zero. This is the outcome of all torrefied materials in this research being gasified under all operational conditions. To put it another way, any torrefied material is not excluded from a certain operating condition. When the relationships between operating parameters and output variables are examined, the steam/fuel ratio is found to be the most influential variable. Temperature and the steam/fuel ratio, not unexpectedly, are positively correlated with power and voltage, but pressure is negatively correlated. These operational parameters have the reverse relationship when it comes to efficiency. Furthermore, there is a negative relationship between the steam/fuel ratio and temperature. The large quantity of steam provided to the reactor can compensate for the lower H_2 production at lower gasification temperatures, or the decreased H_2 production at low steam/fuel ratios can be enhanced by increasing the gasifier temperature. Pressure and other gasifier operating settings have a positive relationship. Because high gasifier temperatures and high steam/fuel ratios can compensate for lower H_2 production at high pressures. The correlations of the output variables with each other were strong. This is not an unusual finding because, as was frequently discussed in the previous sections, the voltage output increased under the operational condition where the power output increased. Efficiency, on the other hand, decreased under operational conditions with increased power and voltage outputs. Additionally, when the correlation between the ultimate analysis results of the torrefied biomass sample and the output variables is investigated, it is determined that carbon is the most dominating variable, followed by oxygen, and hydrogen is the least influential variable. This can be explained by the fact that the hydrogen concentration of solid fuels is relatively uniform (about 5%-6%), implying that there are no substantial variances within fuel types. The correlation map demonstrates that when solid fuel carbon concentration increases, PEM power and voltage outputs improve but efficiency declines. The greater the hydrogen and oxygen concentration of the fuel, on the other hand, provides a better efficiency and the lower the PEM power and voltage outputs. This is a result that is highly compatible with the conclusions reached from Fig. 16 and thereafter. When the relationship between proximate analysis results, which is one of the study's specified input variables, and ultimate analysis results is evaluated, appropriate findings can be obtained. Naturally, the fixed carbon content and the elemental carbon content have a positive relationship. Further, short and long-chain hydrocarbons, aromatic hydrocarbons, carbon monoxide, chlorine and sulfur are common components of volatile matter [85,86]. Thus, a higher volatile matter percentage indicates that the fuel is more oxygen and hydrogen-rich. In contrast, ash has a negative relationship with all three of its elemental carbon, hydrogen, and oxygen. The fixed carbon and volatile matter concentrations decrease as the ash content of the fuel rises, and therefore the carbon, hydrogen, and oxygen concentrations decrease. A similar reasoning can be used to explain the negative correlation between fixed carbon and volatile matter. On a dry basis, the total of volatile matter, ash, and fixed carbon concentrations should be one hundred. When one of these variables grows, it causes the other to decline. Ash content is at relatively low concentrations and is not distributed over a wide range. Therefore, it has a low correlation coefficient with fixed carbon and volatile matter. Changes in volatile matter and fixed carbon content, which make up a substantial percentage of torrefied material, on the other hand, have a considerable impact on each other. There was no substantial relationship between the moisture variable and any of the other variables. However, the moisture variable, as well as the dry basis proximate analysis results, must be chosen as input parameters. Because proximate analysis results for solid materials on a dry basis can be quite similar. Moisture content, on the other hand, may be an important factor in identifying these solid materials from one another. To conclude, although the findings of the proximate analysis do not directly and strongly offer information on the elemental composition, they do provide essential parameters in relation to fuel properties. Proximate analysis findings and operational conditions can be assigned as input variables, and PEM outputs can be predicted, taking into account the technical and statistical reasons given in the section where Fig. 13 is discussed, as well as the information provided by the correlation map.

3.4. Development and assessment of the ANN model

The sensitivity analysis results generated from Aspen Plus simulations were used to create a dataset, and as mentioned before the dataset was adjusted via the data elimination procedure. Ultimately, a dataset including 77,609 of input and output variables was obtained. The Neural Network Toolbox was used to develop, train, test, and validate the ANN model, which was conducted in MATLAB R2021a. The MLP structure was preferred to develop the ANN architecture, which consisted ofi nput, output, and hidden layers. One of the most crucial aspects of building an effective model is splitting data sets so that they should be appropriate for training, testing, and validation. The dataset was randomly divided into three parts: 60% training, 30% testing, and 10% validation. In the training phase, the tangent sigmoid was chosen as the activation function and the Levenberg-Marquardt algorithm as the optimizer. Fig. 16 demonstrates the structure of the ANN developed in this paper.

The input layer has 7 neurons, the first hidden layer has 18 neurons, the second hidden layer has 9 neurons, and the output layer has 3 neurons. Moisture, fixed carbon (db.%), volatile matter (db.%), ash (db.%), gasifier temperature (°C), gasifier pressure (bar), and steam/fuel ratio are all input neurons. Further, power (kW), voltage (V), and efficiency (%) are the output neurons of ANN model. Table 5 summarizes the specifications that belong to the ANN model.

The hyperparameters of the ANN model were adjusted to obtain the lowest mean squared error score as the specified function for training, testing, and validating data sets. The ANN model was trained using randomly selected data, and then test phase was conducted to assess the network's performance using data set that had not been used during the training. Iterations were carried out until the mean squared error value dropped below a certain threshold, resulting in the predicted results with the acceptable accuracy. The R^2 depicts how the estimated and measured values are related. Fig. 17 illustrates a comparison of R^2 values for forecasted and measured values of power, voltage, and efficiency.

Training data is presented in yellow color and testing data is shown in orange color for all output variables. The R^2 values obtained for all output variables are more than 0.99, indicating that the newly developed ANN model can correctly predict PEM parameters for a CFB gasifier/PEM fuel cell system utilizing gasification process input data. Testing R^2 values are slightly lower than training R^2 scores, and plots for all output variables demonstrate a few outliers. Despite this, the ANN

Table 5
Parameters of the ANN model.

PARAMETER	VALUE
The number of artificial neurons in the input layer	7
The number of artificial neurons in the first hidden layer	18
The number of artificial neurons in the second hidden layer	9
The number of artificial neurons in the output layer	3
Type of network and algorithm for network training	Feedforward backpropagation
Transfer function	Tangent sigmoid (TANSIG)
Function of performance assessment	Mean squared error
Optimization algorithm	Levenberg-Marquardt (TRAINLM)
The maximum number of epochs	1000
Number of epochs in which network training was completed	186
Type and percentage of data division (training, test, and validation)	Random, 60%, 30%, and 10%

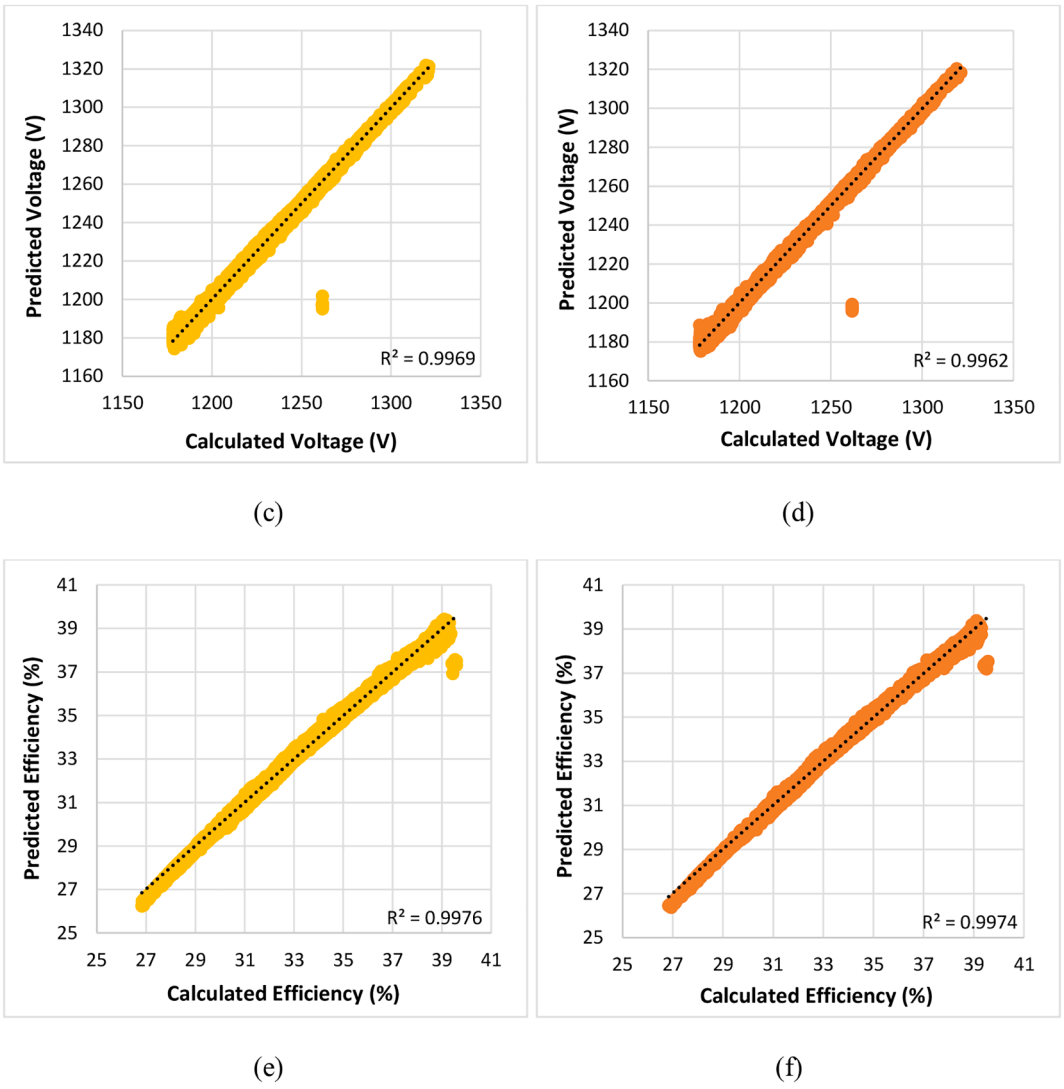

Fig. 17. R^2 results for the output variables (a) power training, (b) power testing, (c) voltage training, (d) voltage testing, (e) efficiency training, (f) efficiency testing.

model's predictive capability is quite satisfactory. When the mean squared error and mean absolute percentage error results, which are considered as performance indicators in addition to R^2, are analyzed, the ANN model's success can be more appreciated. The mean squared error results for the training set's power, voltage, and efficiency outputs were 1.209, 2.655, and 0.017, respectively, while the mean absolute percentage error results were 0.074, 0.075, and 0.285. In addition, the mean squared error results for the testing set's power, voltage, and efficiency outputs were 1.489, 3.269, and 0.018, respectively, while the mean absolute percentage error results were 0.076, 0.076, and 0.287. These metrics, especially with the MAPE value less than 1%, indicate that the newly developed ANN model can accurately predict the PEM fuel cell output parameters for both training and testing.

4. Conclusions

In this paper, a model for a CFB gasifier/steam turbine/PEM fuel cell with Aspen Plus was created. Steam gasification was preferred to produce large amounts of H_2, and the syngas was purified before being fed into the steam turbine system where it receives additional power and cooling. Subsequently, H_2 was supplied into the PEM fuel cell. The CFB gasifier model and the PEM fuel cell model were both validated prior to the parametric investigations. The impact of torrefied material properties, gasifier temperature and pressure, and steam/fuel ratio on PEM fuel cell outputs were discussed in parametric studies. Finally, for a complex integrated system, an ANN model was developed, which was trained with simulation data, to estimate PEM outputs and eliminate complicated equations. This is the first study that investigates the effect of torrefied biomass samples' properties on PEM fuel cell outputs for a sophisticated integrated system dependent on gasification conditions. Moreover, the developed ANN model provides a rapid predictive tool for the integrated system with complicated equations. Additionally, parametric studies assist in determining the proposed new integrated system's minimal operating condition, which is highly dependent on the fuel characteristic. The important findings are as follows:

- High-temperature gasification improves H_2 concentration while increasing syngas LHV and exergy. Gasification at high pressures reduces syngas LHV and exergy while increasing H_2 concentration. The quantity of steam supplied into the reactor is also vital. Syngas LHV and exergy values rise with increasing H_2 concentration, however excessive steam supply lowers syngas quality.
- Parametric studies can help determine which solid fuels can be used in a combined system's gasification process. Depending on the fuel's quality, there are many operating conditions where it cannot produce enough H_2. Poultry litter, one of the 20 different torrefied materials used in this study, was unable to supply enough H_2 for any

of the operating parameters specified in the study, indicating that it is an unsuitable solid fuel for the CFB gasifier/PEM fuel cell system.
- The proximate analysis results showed a random distribution, but the ultimate analysis results, notably the O/C and H/C ratios, revealed a more coherent pattern and were more informative. Power and voltage increased with torrefied material carbonization, but efficiency decreased.
- Increasing the temperature and steam/fuel ratio boosted voltage and power outputs while decreasing efficiency. Contrarily, high pressure increased efficiency while reducing power and voltage. The effect of operating variables on H_2 production rate is directly paralleled by these findings.
- Although there were no substantial correlations between the proximate analysis findings and the PEM outputs, there were correlations between the ultimate analysis parameters. Also, scientific rationale between two analyses indicate that the proximate analysis results can be applied as input variables.
- The ANN model predicts PEM fuel cell output parameters with excellent accuracy based on torrefied biomass proximate analysis and gasification operation parameters ($R^2 > 0.99$ and MAPE 1%). Therefore, performance of systems constructed by the combination of diverse modules and thermochemical processes, such as CFB gasifier/steam turbine/PEM fuel cell plant, can be analyzed using ANN models trained using a dataset of adequate quality and quantity.

Process simulation based on thermodynamic equilibrium, a simplified but effective modeling technique, is a strong tool for providing reliable output and is particularly useful for ANN training. Experimenting with a wide range of operating conditions and fuel types is costly and time-consuming. Importantly, this research offers crucial preliminary data for distinguishing between fuel properties and operating situations. However, the fuel type and operating parameters to be employed in the integrated system can be selected in order to make this research more realistic and suitable to real-world applications, as well as providing a recommendation for future investigations. A more realistic modeling research and data can be created in this setting, taking into consideration reaction kinetics and reactor hydrodynamics. Although such a study would provide more realistic findings in terms of fuel and operating settings, it would fall weak in terms of variables like the assessment of different biochar and operational situations, which we aim to emphasis in our research.

CRediT authorship contribution statement

Furkan Kartal: Data curation, Investigation, Software, Validation, Visualization, Writing – original draft, Writing – review & editing. **Uğur Özveren:** Conceptualization, Data curation, Formal analysis, Funding acquisition, Investigation, Methodology, Project administration, Resources, Software, Supervision, Validation, Visualization, Writing – original draft, Writing – review & editing.

Declaration of Competing Interest

The authors declare that they have no known competing financial interests or personal relationships that could have appeared to influence the work reported in this paper.

Acknowledgements

This work has been supported by Marmara University Scientific Research Projects Coordination Unit under grant number FYL-2020-10139.

References

[1] Narnaware SL, Panwar N. Biomass gasification for climate change mitigation and policy framework in India: A review. Bioresour Technol Rep 2022;17:100892.
[2] Beagle E, Wang Y, Bell D, Belmont E. Co-gasification of pine and oak biochar with sub-bituminous coal in carbon dioxide. Bioresour Technol 2018;251:31–9.
[3] Kartal F, Özveren U. Prediction of torrefied biomass properties from raw biomass. Renewable Energy 2022;182:578–91.
[4] Shankar Tumuluru J, Sokhansanj S, Hess JR, Wright CT, Boardman RD. A review on biomass torrefaction process and product properties for energy applications. Ind Biotechnol 2011;7:384–401.
[5] Chen D, Zheng Z, Fu K, Zeng Z, Wang J, Lu M. Torrefaction of biomass stalk and its effect on the yield and quality of pyrolysis products. Fuel 2015;159:27–32.
[6] Bergman PC, Kiel JH. Torrefaction for biomass upgrading. In: Proc 14th European Biomass Conference, Paris, France. sn2005. pp. 17-21.
[7] Bain RL, Broer K. Gasification. National Renewable Energy Lab. (NREL), Golden, CO (United States); 2011.
[8] Do TX, Lim Y-I, Yeo H, Choi Y-T, Song J-H. Techno-economic analysis of power plant via circulating fluidized-bed gasification from woodchips. Energy 2014;70:547–60.
[9] Vera D, Jurado F, Carpio J, Kamel S. Biomass gasification coupled to an EFGT-ORC combined system to maximize the electrical energy generation: A case applied to the olive oil industry. Energy 2018;144:41–53.
[10] Wright J. Advances in energy technology: the key to sustainability. (1998).
[11] Pinto F, Gominho J, André RN, Gonçalves D, Miranda M, Varela F, et al. Improvement of gasification performance of Eucalyptus globulus stumps with torrefaction and densification pre-treatments. Fuel 2017;206:289–99.
[12] Cerone N, Zimbardi F, Villone A, Strjiugas N, Kiyikci E. Gasification of wood and torrefied wood with air, oxygen, and steam in a fixed-bed pilot plant. Energy Fuels 2016;30:4034–43.
[13] Chen W-H, Chen C-J, Hung C-I, Shen C-H, Hsu H-W. A comparison of gasification phenomena among raw biomass, torrefied biomass and coal in an entrained-flow reactor. Appl Energy 2013;112:421–30.
[14] Couhert C, Salvador S, Commandre J-M. Impact of torrefaction on syngas production from wood. Fuel 2009;88:2286–90.
[15] Chew JJ, Soh M, Sunarso J, Yong S-T, Doshi V, Bhattacharya S. Gasification of torrefied oil palm biomass in a fixed-bed reactor: effects of gasifying agents on product characteristics. J Energy Inst 2020;93:711–22.
[16] Özveren U, Kartal F, Sezer S, Özdoğan ZS. Investigation of steam gasification in thermogravimetric analysis by means of evolved gas analysis and machine learning. Energy 2022;239:122232.
[17] Kartal F, Özveren U. A deep learning approach for prediction of syngas lower heating value from CFB gasifier in Aspen plus®. Energy 2020;209:118457.
[18] Erlach B, Harder B, Tsatsaronis G. Combined hydrothermal carbonization and gasification of biomass with carbon capture. Energy 2012;45:329–38.
[19] Karl J, Pröll T. Steam gasification of biomass in dual fluidized bed gasifiers: A review. Renew Sustain Energy Rev 2018;98:64–78.
[20] Nikrityuk PA, Meyer B. Gasification processes: modeling and simulation. John Wiley & Sons; 2014.
[21] Kartal F, Özveren U. A comparative study for biomass gasification in bubbling bed gasifier using Aspen HYSYS. Bioresour Technol Rep 2021;13:100615.
[22] Paiva MVd. Modeling and simulation of biomass gasification processes; 2020.
[23] Özveren U. Theoretical and experimental investigation of biomass and coal gasification. Marmara Universitesi (Turkey); 2013.
[24] Kuo P-C, Illathukandy B, Wu W, Chang J-S. Plasma gasification performances of various raw and torrefied biomass materials using different gasifying agents. Bioresour Technol 2020;314:123740.
[25] Del Grosso M, Sridharan B, Tsekos C, Klein S, de Jong W. A modelling based study on the integration of 10 MWth indirect torrefied biomass gasification, methanol and power production. Biomass Bioenergy 2020;136:105529.
[26] Kuo P-C, Wu W, Chen W-H. Gasification performances of raw and torrefied biomass in a downdraft fixed bed gasifier using thermodynamic analysis. Fuel 2014;117:1231–41.
[27] Prins MJ, Ptasinski KJ, Janssen FJ. More efficient biomass gasification via torrefaction. Energy 2006;31:3458–70.
[28] Serrano D, Golpour I, Sánchez-Delgado S. Predicting the effect of bed materials in bubbling fluidized bed gasification using artificial neural networks (ANNs) modeling approach. Fuel 2020;266:117021.
[29] Xiao G, Ni M-J, Chi Y, Jin B-S, Xiao R, Zhong Z-P, et al. Gasification characteristics of MSW and an ANN prediction model. Waste Manage 2009;29:240–4.
[30] Szabłowski Ł, Milewski J, Badyda K, Kupecki J. ANN–supported control strategy for a solid oxide fuel cell working on demand for a public utility building. Int J Hydrogen Energy 2018;43:3555–65.
[31] Tian P, Liu X, Luo K, Li H, Wang Y. Deep learning from three-dimensional multiphysics simulation in operational optimization and control of polymer electrolyte membrane fuel cell for maximum power. Appl Energy 2021;288:116632.
[32] Lin Y, Li B, Moiser TM, Griffel LM, Mahalik MR, Kwon J, et al. Revenue prediction for integrated renewable energy and energy storage system using machine learning techniques. J Storage Mater 2022;50:104123.
[33] Sakalis GN. Design and partial load operation optimization of integrated ship energy system based on supercritical CO2 waste heat recovery cycle. Sustain Energy Technol Assess 2022;51.
[34] Pashchenko D. Industrial furnaces with thermochemical waste-heat recuperation by coal gasification. Energy 2021;221:119864.

[35] Shahavi MH, Esfilar R, Golestani B, Sadeghabad MS, Biglaryan M. Comparative study of seven agricultural wastes for renewable heat and power generation using integrated gasification combined cycle based on energy and exergy analyses. Fuel 2022;317:123430.
[36] Behzadi A, Arabkoohsar A, Gholamian E. Multi-criteria optimization of a biomass-fired proton exchange membrane fuel cell integrated with organic rankine cycle/thermoelectric generator using different gasification agents. Energy 2020;201:117640.
[37] Sezer S, Özveren U. Investigation of syngas exergy value and hydrogen concentration in syngas from biomass gasification in a bubbling fluidized bed gasifier by using machine learning. Int J Hydrogen Energy 2021;46:20377–96.
[38] Li J, Xu K, Yao X, Chen S. Prediction and optimization of syngas production from steam gasification: Numerical study of operating conditions and biomass composition. Energy Convers Manage 2021;236:114077.
[39] Sanaye S, Hosseini S. Prediction of blade life cycle for an industrial gas turbine at off-design conditions by applying thermodynamics, turbo-machinery and artificial neural network models. Energy Rep 2020;6:1268–85.
[40] Li B, Gu C-W, Li X-T, Liu T-Q. Numerical optimization for stator vane settings of multi-stage compressors based on neural networks and genetic algorithms. Aerosp Sci Technol 2016;52:81–94.
[41] Sarkar J, Prottoy ZH, Bari MT, Al Faruque MA. Comparison of ANFIS and ANN modeling for predicting the water absorption behavior of polyurethane treated polyester fabric. Heliyon 2021;7.
[42] Long X, Boldrin P, Zhang Y, Brandon N, Paterson N, Millan M. Towards integrated gasification and fuel cell operation with carbon capture: Impact of fuel gas on anode materials. Fuel 2022;318:123561.
[43] Din ZU, Zainal Z. Biomass integrated gasification–SOFC systems: Technology overview. Renew Sustain Energy Rev 2016;53:1356–76.
[44] Beheshti S, Ghassemi H, Shahsavan-Markadeh R. An advanced biomass gasification–proton exchange membrane fuel cell system for power generation. J Cleaner Prod 2016;112:995–1000.
[45] Nguyen HQ, Shabani B. Proton exchange membrane fuel cells heat recovery opportunities for combined heating/cooling and power applications. Energy Convers Manage 2020;204:112328.
[46] Liu Z. Experimental analysis of an integrated biomass gasification and PEM fuel cell system. Energy Sources Part A 2019;41:360–7.
[47] Wahid F, Muslim MB, Saleh S, Samad N. Integrated gasification and fuel cell framework: Biomass gasification case study. ARPN J Eng Appl Sci 2016;11:2673–80.
[48] Detchusananard T, Im-orb K, Ponpesh P, Arpornwichanop A. Biomass gasification integrated with CO2 capture processes for high-purity hydrogen production: process performance and energy analysis. Energy Convers Manage 2018;171:1560–72.
[49] Adefeso IB, Rabiu AM, Ikhu-Omoregbe DI. Refuse-derived fuel gasification for hydrogen production in high temperature proton exchange membrane fuel cell base CHP system. Waste Biomass Valoriz 2015;6:967–74.
[50] Chutichai B, Arpornwichanop A. Performance Improvement of Biomass Gasification and PEMFC Integrated System-Design Consideration for Achieving High Overall Energy Efficiency and Power-to-Heat Ratio Variation. Chem Eng Trans 2015;43:1501–6.
[51] Athanasios L, Nikolaos K, Costas A, et al. Effect of Olive Kernel thermal treatment (torrefaction vs. slow pyrolysis) on the physicochemical characteristics and the CO_2 or H_2O gasification performance of as-prepared biochars. Int J Hydrogen Energy 2021;46(57):29126–41. https://doi.org/10.1016/j.ijhydene.2020.11.230.
[52] Ibrahim RH, Darvell LI, Jones JM, Williams A. Physicochemical characterisation of torrefied biomass. J Anal Appl Pyrol 2013;103:21–30.
[53] Adeleke A, Odusote J, Ikubanni P, Lasode O, Malathi M, Paswan D. The ignitability, fuel ratio and ash fusion temperatures of torrefied woody biomass. Heliyon. 2020;6:e03582.
[54] Bridgeman T, Jones J, Shield I, Williams P. Torrefaction of reed canary grass, wheat straw and willow to enhance solid fuel qualities and combustion properties. Fuel 2008;87:844–56.
[55] Samad NAFA, Saleh S. Analysis of volatile composition released from torrefaction of empty fruit bunch. Mater Today: Proc 2021.
[56] Park J, Meng J, Lim KH, Rojas OJ, Park S. Transformation of lignocellulosic biomass during torrefaction. J Anal Appl Pyrol 2013;100:199–206.
[57] Li J, Zhang X, Pawlak-Kruczek H, Yang W, Kruczek P, Blasiak W. Process simulation of co-firing torrefied biomass in a 220 MWe coal-fired power plant. Energy Convers Manage 2014;84:503–11.
[58] Berrueco C, Recari J, Güell BM, Del Alamo G. Pressurized gasification of torrefied woody biomass in a lab scale fluidized bed. Energy 2014;70:68–78.
[59] Yang Z, Sarkar M, Kumar A, Tumuluru JS, Huhnke RL. Effects of torrefaction and densification on switchgrass pyrolysis products. Bioresour Technol 2014;174:266–73.
[60] Eseltine D, Thanapal SS, Annamalai K, Ranjan D. Torrefaction of woody biomass (Juniper and Mesquite) using inert and non-inert gases. Fuel 2013;113:379–88.
[61] Hu J, Song Y, Liu J, Evrendilek F, Buyukada M, Yan Y, et al. Combustions of torrefaction-pretreated bamboo forest residues: Physicochemical properties, evolved gases, and kinetic mechanisms. Bioresour Technol 2020;304:122960.
[62] Atimtay A, Yurdakul S. Combustion and Co-Combustion characteristics of torrefied poultry litter with lignite. Renewable Energy 2020;148:1292–301.
[63] kumar Singh R, Sarkar A, Chakraborty JP. Effect of torrefaction on the physicochemical properties of pigeon pea stalk (Cajanus cajan) and estimation of kinetic parameters. Renewable Energy 2019;138:805–19.
[64] Barzegar R, Yozgatligil A, Olgun H, Atimtay AT. TGA and kinetic study of different torrefaction conditions of wood biomass under air and oxy-fuel combustion atmospheres. J Energy Inst 2020;93:889–98.
[65] Van Krevelen D. Coal, 3rd complementary. revised ed. Amsterdam: Elsevier; 1993.
[66] Ahmad M, Subawi H. New Van Krevelen diagram and its correlation with the heating value of biomass. J Agric Environ Manage 2013;2:295–301.
[67] P. Basu. Biomass gasification, pyrolysis and torrefaction: practical design and theory. Academic press; 2018.
[68] Huang W, Zheng D, Chen X, Shi L, Dai X, Chen Y, et al. Standard thermodynamic properties for the energy grade evaluation of fossil fuels and renewable fuels. Renewable Energy 2020;147:2160–70.
[69] Zhang Y, Ji Y, Qian H. Progress in thermodynamic simulation and system optimization of pyrolysis and gasification of biomass. Green Chem Eng 2021;2:266–83.
[70] Shabbar S, Janajreh I. Thermodynamic equilibrium analysis of coal gasification using Gibbs energy minimization method. Energy Convers Manage 2013;65:755–63.
[71] Jung SY, Nguyen TV. An along-the-channel model for proton exchange membrane fuel cells. J Electrochem Soc 1998;145:1149.
[72] Nagajothi S, Elavenil S. Influence of aluminosilicate for the prediction of mechanical properties of geopolymer concrete–artificial neural network. Silicon 2020;12:1011–21.
[73] Uddin MN, Li L-Z, Ahmed A, Almajhali KYM. Prediction of PVA fiber effect in Engineered Composite cement (ECC) by Artificial neural Network (ANN). Mater Today: Proc 2022.
[74] M.A. Sahraei, M. Kayaci Çodur. Prediction of Transportation Energy Demand by Novel Hybrid Meta-Heuristic ANN. Available at SSRN 3931666.
[75] Verhage AJ, Coolegem JF, Mulder MJ, Yildirim MH, de Bruijn FA. 30,000 h operation of a 70 kW stationary PEM fuel cell system using hydrogen from a chlorine factory. Int J Hydrogen Energy 2013;38:4714–24.
[76] Guandalini G, Foresti S, Campanari S, Coolegem J, ten Have J. Simulation of a 2 MW PEM fuel cell plant for hydrogen recovery from chlor-alkali industry. Energy Procedia 2017;105:1839–46.
[77] Singh DK, Tirkey J. Process modelling and thermodynamic performance optimization of biomass air gasification fuelled with waste poultry litter pellet by integrating Aspen plus with RSM. Biomass Bioenergy 2022;158:106370.
[78] Ramzan N, Ashraf A, Naveed S, Malik A. Simulation of hybrid biomass gasification using Aspen plus: A comparative performance analysis for food, municipal solid and poultry waste. Biomass Bioenergy 2011;35:3962–9.
[79] Kombe EY, Lang'at N, Njogu P, Malessa R, Weber C-T, Njoka F, et al. Numerical investigation of sugarcane bagasse gasification using Aspen Plus and response surface methodology. Energy Convers Manage 2022;254.
[80] Vikram S, Rosha P, Kumar S, Mahajani S. Thermodynamic analysis and parametric optimization of steam-CO2 based biomass gasification system using Aspen PLUS. Energy 2022;241.
[81] Shen L, Gao Y, Xiao J. Simulation of hydrogen production from biomass gasification in interconnected fluidized beds. Biomass Bioenergy 2008;32:120–7.
[82] Ku X, Li T, Løvås T. Eulerian-Lagrangian simulation of biomass gasification behavior in a high-temperature entrained-flow reactor. Energy Fuels 2014;28:5184–96.
[83] Sezer S, Kartal F, Özveren U. Prediction Of Chemical Exergy Of Syngas From Downdraft Gasifier BY Means Of Machine Learning. Therm Sci Eng Progr 2021:101031.
[84] Klasson KT. Biochar characterization and a method for estimating biochar quality from proximate analysis results. Biomass Bioenergy 2017;96:50–8.
[85] Wang T. In: Integrated Gasification Combined Cycle (IGCC) Technologies. Elsevier; 2017. p. 1–80.
[86] Z. Ilham. Biomass classification and characterization for conversion to biofuels. Value-Chain of Biofuels. Elsevier; 2022. pp. 69-87.